A DNAmRep epigenetic fingerprint for determining cellular replication age

Christopher Minteer[1], Marco Morselli[2], Margarita Meer[1], Jian Cao[1,3], Sabine Lang[1], Matteo Pellegrini[2], Qin Yan[1], Morgan Levine[1].

[1]Department of Pathology, Yale School of Medicine, New Haven, CT, USA 06519
[2]Department of Molecular, Cell, and Developmental Biology, University of California Los Angeles, Los Angeles, CA, USA 90095
[3]Rutgers Cancer Institute of New Jersey, New Brunswick, NJ, USA 08901.

Abstract:

Aging is known to elicit dramatic changes to DNA methylation (DNAm). However, the causes and consequences of such alterations to the epigenome remain unclear. Therefore, the utility of biomarkers of aging based on DNAm patterns will depend on our ability to link them to cellular features, such as proliferation, differentiation, transcriptional repression/activation, senescence, and transformation. Using DNAm from serially passaged mouse embryonic fibroblasts (MEFs), we developed a predictor of replication that is able to accurately predict passage number in independent sample. Our measure, termed DNAmRep, was shown to strongly increase with age when examined in multiple tissues (blood, liver, kidney, lung and adipose). Furthermore, we observed replicative deceleration in animal undergoing caloric restriction. Upon reprogramming to iPSCs, cells derived from both lung and kidney fibroblasts exhibited resetting of our DNAmRep measure. This measure also increased in response to differentiation among B-cell populations. Enrichment analysis implicated CBX7, RNF2 and HDAC2 as potentially important transcription factors and chromatin regulators in the DNAm replication signature. Finally, DNAmRep correlated with beta-galactosidase activity in replicative senescent MEFs, but not in radiation or drug induced senescent MEFs, and was partially separated by immortalization with Large T antigen K1 mutant (LTK1), suggesting that it reflects mitotic history, rather than senescent state. Overall, this study identifies mitotically-derived alterations to the methylome, which partially underlie known epigenetic aging phenomena.

This is a preliminary report of work that has not been certified by peer review.

Introduction:

Aging is characterized by a progressive decline in cell, tissue and organ integrity that manifests as age-related diseases and ultimately death [1,2]. Telomere attrition [3], cellular senescence [4-6], DNA damage [7], stem cell exhaustion [8] and epigenetic modifications [9] represent just a few molecular and cellular features of the aging process. While these hallmarks have been extensively investigated, their interactions and the resulting emergence that leads to the failure of the organism is not well characterized. The study of epigenetic alterations in aging represents an exciting opportunity to investigate the connections between various hallmarks given that changes to DNA methylation and/or histone modifications have been shown to traverse various molecular and cell changes observed in aging.

DNA methylation (DNAm) refers to the addition of a methyl group (CH3) to a CpG dinucleotide (5'—C—phosphate—G—3'). In most cases, DNAm is associated with transcriptional repression via its effect on chromatin organization, and is thought to control a number of cellular properties, including differentiation [10], replication [11], X-inactivation [12], stress response [13], and genomic imprinting [14]. Initially, *de novo* methyltransferases establish methylation patterns that are necessary for organismal development [15,16]. These patterns are then modulated by maintenance methyltransferases over the course of the lifespan [17,18] during which, subtle changes can dramatically alter promoter function [19-21] and distal regulatory elements [22,23]. Interestingly, changes in DNAm with aging were first reported more than three decades ago [24]. These changes depict a specific pattern characterized by a gain of DNAm at gene promotors and loss of global DNAm, representing trends towards hypomethylation in intergenic regions associated with dispersed retrotransposons, heterochromatic DNA repeats, and endogenous retroviral elements [25]. Given the predictability of these age-related changes, researchers began applying machine learning techniques to develop age predictors from DNAm that could serve as biomarkers of aging. To date, these so called "epigenetic clocks" have been applied in a plethora of tissues across diverse mammalian species and have been shown to be predictive of lifespan and healthspan, above and beyond chorological age [26-30]. However, there is a growing emphasis in the field that we need to shift the focus to understanding exactly what age-related patterns in DNAm are capturing.

To address a common cellular feature in all tissues we turned to the nearly 60 old idea of exhaustive replication [31-33]. Hayflick and others noticed that normal human fetal cells could passage between 40-60 times before entering a senescent state of growth arrest [34]. Previous studies have linked replication and cell cycle dynamics to changes in DNAm [35-37], but it is unclear whether the DNAm changes occurring from one passage to the next could reflect aging at the level of the cell, which may ultimately manifest as age-related declines in tissues, organs, and the organism as a whole.

The aim of this paper is to develop a biomarker of aging by modeling the dynamic DNAm changes as a function of replicative aging in cells. In doing so, our goal was to determine the extent cellular turnover plays in epigenetic aging and also elucidate key CpG regions,

This is a preliminary report of work that has not been certified by peer review.

binding factors and chromatin regulators of cellular replication that could be used to determine drivers of the aging process and assess productive anti-aging therapies in the future.

This is a preliminary report of work that has not been certified by peer review.

Results:

Developing a replication based DNAm biomarker:

To explore replicative aging and understand its association with DNA methylation, we derived a primary mouse embryonic fibroblast culture system that was exhaustively passaged (Figure 1A, Supplemental Figures 1A-D). DNAm was assessed at each passage in three biological replicates via reduced representation bisulfite sequencing (RRBS). The primary data used to train the replication predictor, termed DNAmRep, was obtained from passage 1-6 of the culture MEF system. Of the three MEF cell lines, replicates MEF1 and MEF2 were used in training and MEF3 was used for validation. In both cases, passages 5 and 6 were combined to make passage 5.5 due to low DNA content prior to RRBS sequencing.

Prior to training DNAmRep, we conducted principal component analysis (PCA) to visualize variance by passage to ensure each replicate (MEF1-3) was capturing similar replicative phenotypes and that there was clear directionality as passage increased (Figure 1B). PCA1-4 captured greater than 70% of variance, with PCA1 and PCA2 demonstrating linear association with passage number (Figure 1B, Supplemental Figure 1E). We determined there was no need to correct for batch error prior to implementing supervised machine learning.

Based on the MEF data, we used a supervised machine learning approach (elastic net regression) to generate a classifier of replication or DNAmRep. Pooling MEF1 and MEF2 passaged cells, we used samples at passage 1 (N=2), passage 2 (N=1), passage 3 (N=2), passage 4 (N=2) and passage 5.5 (N=2) to train a linear predictor of DNAmRep (Figure 2A). In anticipation of validating DNAmRep in robust *in vivo* data sets we sub-selected common CpGs between our MEF data, Petkovich et. al 2017 [38] and Thompson et. al 2018 [39] to generate 28,323 common CpG sites. Based on our previous observations that combining PCA with elastic net yields more robust epigenetic age measures [DNAmSen], we applied a similar strategy here. PCA was conducted on the 28,323 common CpGs using the training samples (total N=9). PCs1-40 were then fed into the elastic net penalized regression (gaussian distribution) to generate a linear predictor of passage number. Six PCs were selected by the penalized regression approach based on 10-fold cross-validation (PC2, PC4, PC6, PC8, PC9 and PC29) (Supplemental Figure 2). Overall, this method uses all 28,323 CpG sites, but assigns loading coefficients to each CpG based on the PCA to calculate a final score, from now on considered DNAmRep.

In vitro validation and gene enrichment analysis confirms replicative origins:

The robustness of DNAmRep and the mechanistic insights generated from the marker was determined based on key validation data to ensure the signal was in fact occurring from cellular replication and aging. As validation, we first calculated DNAmRep in our testing samples for passages 1, 2, 3, 4 and 5.5 from MEF3 and report cor=0.83 (p=0.041), validating that the marker is in fact progressively capturing a replicative “ticking” effect (Figure 2B). The decrease in correlation was shown to result from a leveling off or

This is a preliminary report of work that has not been certified by peer review.

reversion in passage 5.5 cells, which could be due either to our pooling of passage 5 and 6 in the training samples or to a non-linearity at later replicative stages. However, additional samples will be needed to determine the cause.

To determine exactly what DNAmRep is capturing, we investigated the CpG compositions of the highest loading CpGs in each selected PC comprising the final marker (Loading coefficient>0.02) (Supplemental Figure 2B-D). Genomic partition and chromosome distribution plots demonstrate that the selected CpGs (N=3087) are equally distributed across the entire genome and are not clustered in specific chromosomes or regions (Supplemental Figure 2C-D). However, genome enrichment analysis using Cistrome does identify enriched chromatin regulators and transcription factors that have significant overlap with the selected CpG sites (Supplemental Figure 2E-G). Using the original 28,323 CpG sites as a reference/background (Supplemental Figure 2E) and selecting the most significant genes, we generated Venn diagrams and string plots of the resulting hits and also categorized each gene by function (Figure 2C-E). We report known cell cycle, replication and age associated transcription factors (TFs) like HDAC2, RNF2, C17orf96, CXCC1, MYC and CBX7 and processes like cellular processing, metabolic processing and biological regulation as key components of DNAmRep (Figure 2C-E). Our enrichment results further suggest DNAmRep is capturing biological networks of cellular replication and aging.

<u>In vivo validation and investigation into anti-aging therapies:</u>

We next examined DNAmRep for tissue specificity and predicting anti-aging effects from caloric restriction (CR) and Rapamycin treatment. Using three aged samples (2, 10 and 20 months) from C57BL/6J mice in Thompson et. al 2018, we determined that DNAmRep significantly increases with age in lung, liver, adipose, blood and kidney tissue with greatest correlation occurring in liver (cor=0.59, p=7e-0.7) (Figure 3A). We next calculated DNAmRep in a blood dataset from Petkovich et. al 2017 that included C57BL/6J mice between 20-1050 days and found DNAmRep correlated with age with r=0.69 (p=1.6e-23). Using this same data, we also found that DNAmRep was reduced in CR mice relative to controls (p=0.00259), perhaps highlighting replicative slowing from dietary intervention (Figure 3B). Finally, in the same dataset we determined DNAmRep also exhibits a significant decrease in kidney and lung fibroblasts upon reprogramming to induced pluripotent stem cells (iPSCs) (p=0.05) (Figure 3C).

Next, using data from Cole et. al 2017 [40], we investigated if DNAmRep could predict replicative deceleration in liver tissue from Rapamycin treatment. Since there was only 321 overlapping CpGs with Cole et. al 2017 and DNAmRep, and that DNAmRep marginally correlated with MEF3 validation (cor=0.187), we retrained DNAmRep using the same MEF training and validation data but using the overlapped CpGs from our original 472k CpGs and Cole et. al 2017 to achieve a more robust marker with cor=0.9 (p=0.014) from 3465 overlapped CpGs (Supplemental Figure 3A). Even with retraining DNAmRep, we found that DNAmRep was not associated with Rapamycin treated C57BL/6J mice at 22 months (p=0.77), although it did capture general age-related changes between old samples (22 months) and young controls (2 months) (p=0.043)

This is a preliminary report of work that has not been certified by peer review.

(Figure 3D). With only 4 samples in each group, higher powering and more samples are likely required to determine the replicative effects of Rapamycin treatment.

Finally, we expanded the reach of DNAmRep to test if it could distinguish splenic B-cell differentiation (0-8 divisions) [41]. Barwick et. al 2016 investigated the role of DNAm during plasma cell differentiation. They labeled splenic $B220^{+}$ $CD43^{-}$ cells from naïve C57BL/6J mice with carboxyfluorescein succinimidyl ester (CFSE), injected them into uMT (B-cell deficient) mice and after 24h challenged with lipopolysaccharide (LPS) to induce divisions and differentiation. We were interested in the RBBS data generated from Divisions 0, 1, 3, 5 and 8 to conclude if DNAmRep captured dynamic changes in replication. Again, due to low CpG overlap (604) and correlation with MEF3 validation (cor=-0.156), we retrained DNAmRep with the 2331 overlapped CpGs from the original 472k CpGs and Barwick et. al 2016. The new measure more accurately predicted MEF3 with cor=0.78 (p=0.067) (Supplemental Figure 3B). Of note, DNAmRep detected terminal differentiation at division 8 from CD138+ sorted samples, again confirming the measure approximates replicative history (Figure 4). We conclude DNAmRep captured the expansion of the differentiation process (cor=0.60, p=0.018), suggesting the marker may be capturing a general age related “ticking” that occurs as cells transition from an embryonic and naïve state to an aged and mature cellular state (Figure 4).

As a control, we compared DNAmRep to average DNAm in all datasets. We confirm DNAmRep is capturing true biological variance and not simply global changes in methylation (Supplemental Figure 4). Most importantly, there is no correlative directionality in the original training and validation MEF data (cor=0.3, p=0.28) (Supplemental Figure 4A). As well, we used elastic net regression on the N=9 passaged MEF samples within the sub-selected CpGs without PCA to generate a 44 CpG predictor (Supplemental Figure 5). Of note, the marker generated using just 44 CpGs displayed cor=0.99 (p=0.00015) for MEF3 validation and captured similar TFs like CBX7 and HDAC2 from genome enrichment analysis, providing additional evidence that the training data is robust and likely capturing biological components of cellular replication (Supplemental Figure 5).

<u>Distinguishing senescence from replicative signals:</u>

Replicative exhaustion is a robust inducer of cellular senescence. Therefore, we considered the possibility that our DNAmRep signature was capturing the increasing proportion of senescent cells with each passage, rather than a signature of mitotic history. To test this, we assayed beta-galactosidase (β-gal) activity—the most validated senescence biomarker—at each passage (Supplemental Figure 1B-D). In addition, we induced senescence using irradiation, doxorubicin and etoposide in three additional MEF cell lines (MEF4-6) and conducted RRBS in the same batch as the training and validation data for DNAmRep (Supplemental Figure 6). Our results showed that DNAmRep did not correlate with β-gal activity in irradiated or drug induced senescent cells (cor=0.0086, p=0.74) (Figure 5A), but did marginally correlate with β-gal activity of replicative senescence samples (cor=0.4, p=0.29) (Figure 5B). We then analyzed the replicative senescence data by passage number, which increased DNAmRep significance to

This is a preliminary report of work that has not been certified by peer review.

cor=0.55 (p=0.08) (Figure 5C), suggesting DNAmRep is predominately capturing passage based mitotic changes in methylation. We also considered that DNAmRep may also capture certain programs of replicative senescence. To determine the extent replicative senescence contributes to DNAmRep, we immortalized MEFs with LTK1 to suppress p53 as reported previously [42] (Figure 5D). Immortalized and control cells were all aged for 5 passages. We report suppressed β-gal activity in LTK1 transfection compared to aged controls, confirming p53 suppression and replicative maintenance (Figure 5D). When assaying DNAmRep score in immortalized (non-senescent) vs. old (senescent) control populations we observed marginally greater replicative capacity (p=0.35) in immortalized cells (Figure 5E). Altogether, these results suggest replicative, like drug and irradiation induced senescence, are not prominent drivers of DNAmRep, although additional experiments are required to quantitate senescence vs. replicative capacity and any overlap that exists. Our data supports the conclusion that DNAmRep detects biological changes occurring from cellular replication and exhaustive passaging, but not from general damage occurring independent of cellular lifespan.

This is a preliminary report of work that has not been certified by peer review.

Discussion:

Consistent evidence supports the notion that DNA methylation is dramatically altered with aging [32]. While numerous clocks have been derived from these changes, it remains unclear as to what age-related processes or mechanisms drive epigenetic aging. We aimed to determine a unique cellular feature that likely drives some of the age-related alterations in DNAm captured in clocks. Instead of training a penalized regression model to predict chronological age, we deployed a bottom-up approach in which we identify the DNAm signals of a specific age-related trait—cell replication—and then tested whether it recapitulated the epigenetic aging changes reported in various tissues and biofluids.

By exhaustively replicating primary MEFs, we trained a DNAm predictor of passage number, called DNAmRep and demonstrate that it not only accurately estimates replication passage (Figure 2B), but also tracks age in multiple tissues (Figure 3A), is modifiable by dietary intervention (Figure 3B), and exhibits resetting upon reprogramming to pluripotency (Figure 3C). For instance, we found that DNAmRep measured in whole blood of C57BL/6 mice was correlated with age at r=0.69 (Figure 3B). Additionally, similar to existing epigenetic clocks, DNAmRep exhibited non-linear age increases, such that it showed sigmoidal trends with accelerated aging during development followed by a slower and more linear increase after about 150 days, with exponential increases at late life, perhaps indicative of oncogenicity. Overall, this likely reflects increased mitotic rates during growth and development that slow after reaching maturity (estimated to be around 4-6 months in a mouse) and increase during diseases like cancer [43-46].

DNAmRep also exhibited age-related increases in lung, liver, adipose, blood and kidney tissue. However, it did not correlate significantly with age in muscle (Figure 3A). Liver showed the strongest age correlation (cor=0.59) and both liver and blood exhibited the highest values from DNAmRep. This may reflect the higher proliferative capacity of cells in these samples [47,48]. Muscle also showed higher DNAmRep overall, but did not significantly increase with age. This may reflect the fact that muscle grows fairly rapidly during development [49], but that adult skeletal muscle tends to be comprised of largely postmitotic cells [50]. While additional experiments will help characterize epigenetic signatures of replication and regenerative capacity of tissues and cells, our results suggest DNAmRep is capturing general growth-based phenotypes common across many tissues.

While it is important to develop biomarkers than enable researchers to track aging changes *in vivo* and *in vitro*, the ultimate goal is to develop measures that are also modifiable to intervention. Using DNAm assessed in blood, we report that DNAmRep shows response to CR, suggesting that CR may slow mitotic rate in blood. CR is known to downregulate the insulin/IGF1 pathway [51]. Importantly, IGF1 is a growth factor that stimulates cell proliferation and can promote cancer via inhibition of apoptosis [52,53]. Interestingly, CR, without malnutrition, has also been shown to reduce cancer incidence and progression in mice [54,55]. Our results suggest that CR could be acting via slowing cell turnover. Additionally, our results showed that the longer mice underwent CR, the more they diverged from normal controls on the basis of DNAmRep. This could suggest

This is a preliminary report of work that has not been certified by peer review.

that prolonged CR does not simply decrease, or reverse epigenetic aging temporarily, but rather decelerates it by slowing proliferation over time.

We also report replicative renewal in lung and kidney fibroblasts following reprogramming to iPSCs, supporting the conclusion that DNAmRep can not only be slowed, but actually reversed (Figure 3C). For instance, both lung and kidney fibroblasts were predicted to be equivalent to cells passaged just over 3 times, while all iPSC derivatives were predicted approximate cells at passage 1. This suggests that the major epigenetic changes acquired during replication can be reset to some extent. While reprogramming represents an exciting regenerative prospect in the aging field, some issues remain—namely the propensity for incidence of teratomas when reprogramming is conducted *in vivo* [56,57]. However, partial reprogramming without dedifferentiation may provide a path forward and it will be important to determine whether resetting of the replication signature also occurs under those circumstances.

To better understand what DNAmRep was capturing, we preformed enrichment analysis to identify functional mechanisms driving DNAm alterations during proliferation. A number of transcription factor binding sites were found to be enriched in regions comprised of the CpGs that drove our DNAmRep signature. Upon further investigation of these TFs, we found that many are related to cellular processing, metabolic processing, biological regulation, and are intricately involved in development, replication and aging (Figure 2E). CpGs proximal to CBX7 binding motifs were over represented in 4 of 6 PCs, whereas those proximal to RNF2 were over represented in 5 or 6 PCs (Figure 2C). CBX7 is a known regulator of cellular lifespan through the p16/Rb and p19/p53 pathways [58]. Furthermore, CBX7 can induce self-renewal and has been used as a tool to extend lifespan and induce immortalization in culture systems by suppressing key tumor suppressors and allowing the cell to escape senescence [58,59]. It is unclear exactly how CBX7 functions with age, but considering CBX7 is downregulated by replicative senescence maintenance, CBX7 activity likely declines with age as senescence accumulates. Additional evidence suggests CBX7 may initiate H3K9me3 formation at the p16 promoter, further supporting its role in cellular suppression and growth [60].

Additionally, both RNF2 and HDAC2 showed enrichment for binding near the selected CpGs and have both been previously shown to regulate cell cycle proliferation via p53 [61,62]. RNF2 is an E3 ligase that can target p53 for degradation [60], while HDAC2 suppresses p53 activity via deacetylation. Additionally, multiple studies have demonstrated that HDAC2 inactivation can result in a senescence like G1 arrest [62]. Overall, the genes, chromatin regulators and repressive elements found to be enriched in our signature further support the notion that DNAmRep is capturing replicative features of the aging process, such as cellular regulation, expansion and growth. We conclude that our strategy to not repress any of the initial 28,323 CpGs included in DNAmRep, and selecting significance based on loading coefficients, allows greater biological influence over non-PCA trained methods (Supplemental Figure 5).

This is a preliminary report of work that has not been certified by peer review.

We next applied DNAmRep in two additional datasets [40,41] to explore if Rapamycin treatment resulted in replicative deceleration and then if the measure could expand in a splenic B cell differentiation model. In each dataset, CpG overlap was low, thus we retrained DNAmRep and used MEF3 to validate the associated measures (Supplemental Figure 4). In Cole et. al 2017, we determined Rapamycin did not slow epigenetic replication speed (p=0.77), although age-related changes were detected (p=0.043) (Figure 3D). With only 4 samples in each group, detection power may be limited. Although Rapamycin treatment was not significant, many reports implicate Rapamycin as an anti-aging therapy [63]. Larger longitudinal cohorts are required to determine the extent Rapamycin influences replicative capacity.

In our final comparison, we were intrigued with a series of recent studies that demonstrated B cell activation, which requires cellular division, was linked to DNA hypomethylation [41,64]. Barwick et. al 2016 demonstrated that demethylation first occurred at the transcription factors NF-KB and AP-1 and then later at IRF and Oct-2, suggesting cell division dependent activation [41]. Follow-up analysis revealed that *de novo* methylation can also limit B cell activation [64], thus we considered if DNAmRep could also capture this coordinated hypomethylation state of cellular activation. DNAmRep successfully differentiated B cell activation by division (1-8) (cor=0.60, p=0.018). We also confirm division correlated with mean DNAm (cor=-0.83, p=2e-5) (Supplemental Figure 4E). We conclude that DNAmRep can capture division-coupled epigenetic remodeling in a diversity of cell programs, highlighting replication as an important factor in epigenetic aging.

Finally, to confirm DNAmRep was in fact capturing features of cellular replication and not general damage from senescence phenotypes, we compared DNAmRep to replicative, drug and irradiation induced senescence states in MEFs (Figure 5, Supplemental Figure 6). We previously reported a senescence trained epigenetic marker, DNAmSen, that was trained from replicative, irradiation and oncogene induced senescence states in human fibroblasts and mesenchymal stromal cell and presented robust correlations with age and disease status [65], thus we were interested in overlap between DNAmRep and senescence states. We hypothesized that if DNAmRep was truly capturing mitotic ticking and not senescence, then senescence activity would not correlate with DNAmRep outcome. Our results demonstrate DNAmRep does not predict cellular senescence when compared by senescence status (Beta-galactosidase activity) for passage independent senescence samples (irradiation and drug induced) (cor=0.088, p=0.74). Replicative senescence samples were marginally correlated (cor=0.4 p=0.29) (Figure 5A-B) and when analyzing the samples by passage, DNAmRep better predicted the replication outcome (cor=0.55, p=0.08) (Figure 5C). From this initial analysis we conclude DNAmRep is primarily capturing replication based epigenetic changes and not DNA damage-based senescence programs associated with acute damage. We next immortalized cells with LTK1 to inactivate p53, leading to reduced senescence accumulation compared to passaged matched controls (Figure 5D). Importantly, p53 and/or Rb inactivation are sufficient for murine fibroblast immortalization [66-68]. The marginal replicative ticking captured by DNAmRep in old (senescent) vs. immortalized (non-senescent) samples is likely the underlying tumor suppression occurring from LKT1 transformation. Of note,

This is a preliminary report of work that has not been certified by peer review.

chromatin binding factors like RNF1, which was enriched in DNAmRep, are a direct modulator of p53 status, providing a potentiation explanation for the increased DNAmRep score in immortalized vs. passage control cells (p=0.35) (Figure 5E). We conclude DNAmRep is not capturing or driven by senescence phenotypes, although further replication of immortalized samples would help decipher the exact role replicative senescence plays in DNAmRep. Overall, our results suggest cellular replication is a driver of epigenetic aging process and that DNAmRep can predict cellular lifespan and differentiate anti-aging interventions, advocating use in future mouse aging studies.

This is a preliminary report of work that has not been certified by peer review.

Conclusion:

We report a novel mouse epigenetic predictor of cellular replication, termed DNAmRep, that accurately predicts cellular lifespan and passage in culture. Moreover, DNAmRep shows significant increase with age in blood, liver, kidney, lung and adipose tissue *in vivo*. We provide evidence for potential modifiability in the form of deceleration of the age-associated increased in DNAmRep in response to CR and a resetting of DNAmRep in kidney and lung fibroblast upon re-programming to iPSCs. DNAmRep is well represented across the entire mouse genome and genomic enrichment analysis from variable CpGs highlight potential key age-related drivers like CBX7, RNF2 and HDAC2. Surprisingly, DNAmRep also predicts age-related hypomethylation established in B cell differentiation and is highly correlated with each subsequent division. Finally, our results suggest that DNAmRep is not capturing senescence programs independent of passage, but may be in part driven by replicative senescence phenotypes. Overall, this study implicates cellular replication as a key driver of epigenetic aging and highlights the need to develop epigenetic age measures using bottom-up approaches that capture key aging processes.

Acknowledgments:

This work was funded by support by the Glenn Foundation (award for Research in Biological Mechanisms of Aging) and the National Institute on Aging (R01AG068285 and R01AG065403).

Competing interests:

No competing interests to report.

This is a preliminary report of work that has not been certified by peer review.

Figures:

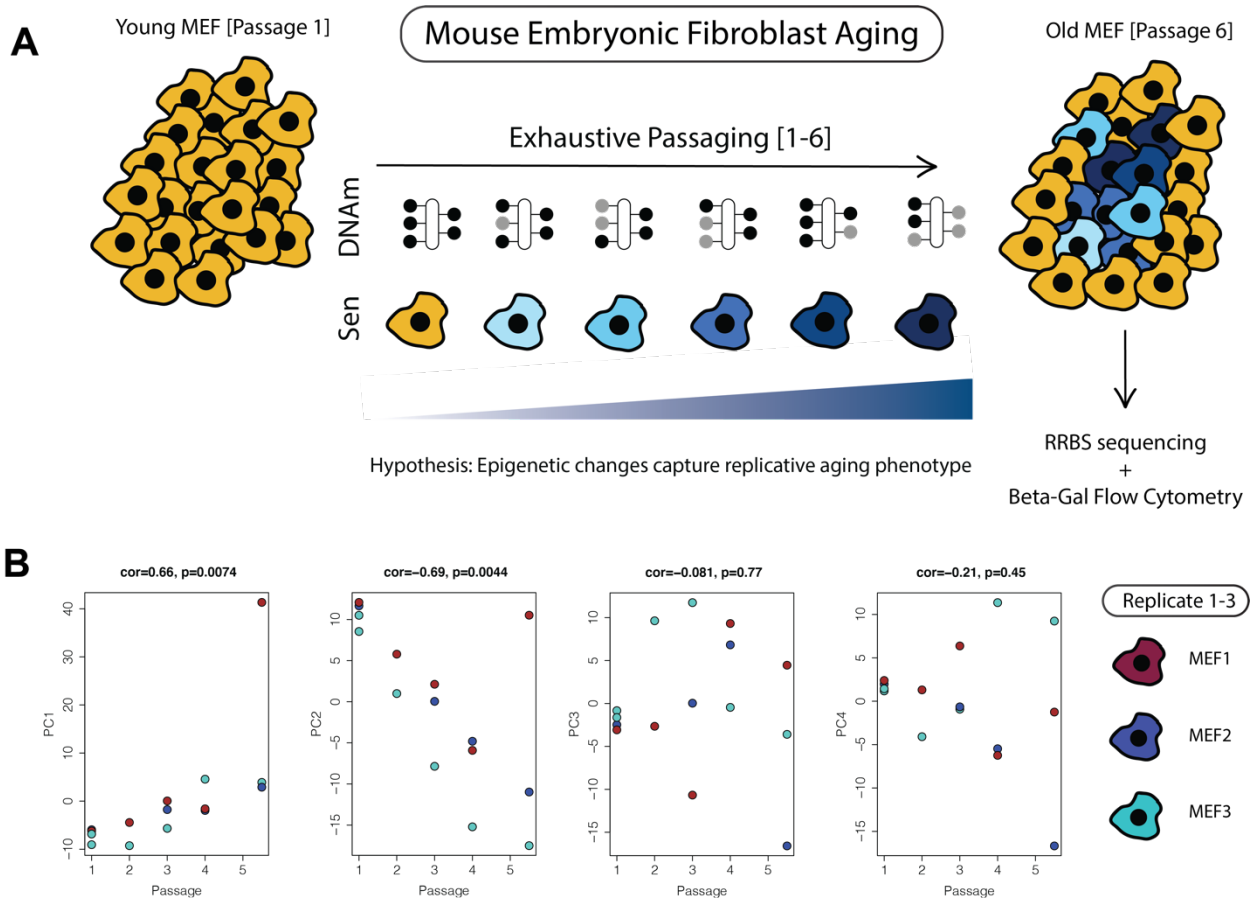

Figure 1: Principal component analysis of replicative aging in mouse embryonic fibroblasts. (A) MEF aging schematic demonstrating senescence accumulation and epigenetic programing with passage/age. (B) Principal component analysis of all MEF cell lines used for training (MEF1-2) and validating (MEF3) DNAmRep. Note, passage 5 and 6 were combined due to low DNA content prior to RRBS sequencing.

This is a preliminary report of work that has not been certified by peer review.

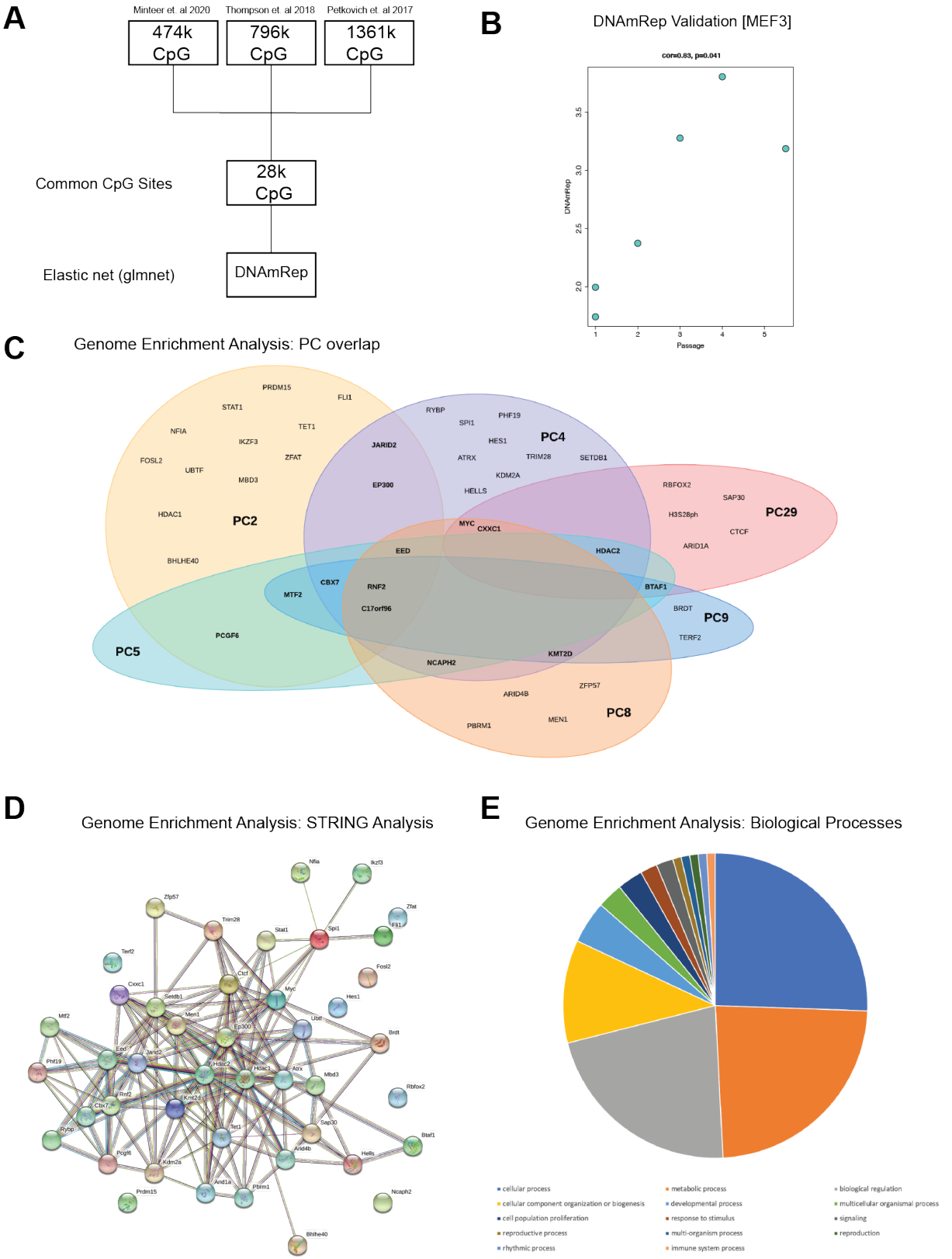

This is a preliminary report of work that has not been certified by peer review.

Figure 2: A DNAm replication-based clock (DNAmRep) captures passaging based cellular phenotype and is enriched in genes related to cellular processing. (A) Flow chart displaying selection of 28,323 common CpG sites between MEF data (474k) and *in vivo* validation datasets. (B) Replication validation of DNAmRep using MEF3. (C) Venn diagram of significant driver genes (transcription factors and chromatin regulators) determined via gene enrichment analysis and sorted by PC from DNAmRep elastic net regression model. (D) STRING analysis of driver genes from genome enrichment analysis in DNAmRep from (C). (E) Categorized gene function analysis of driver genes from (C).

This is a preliminary report of work that has not been certified by peer review.

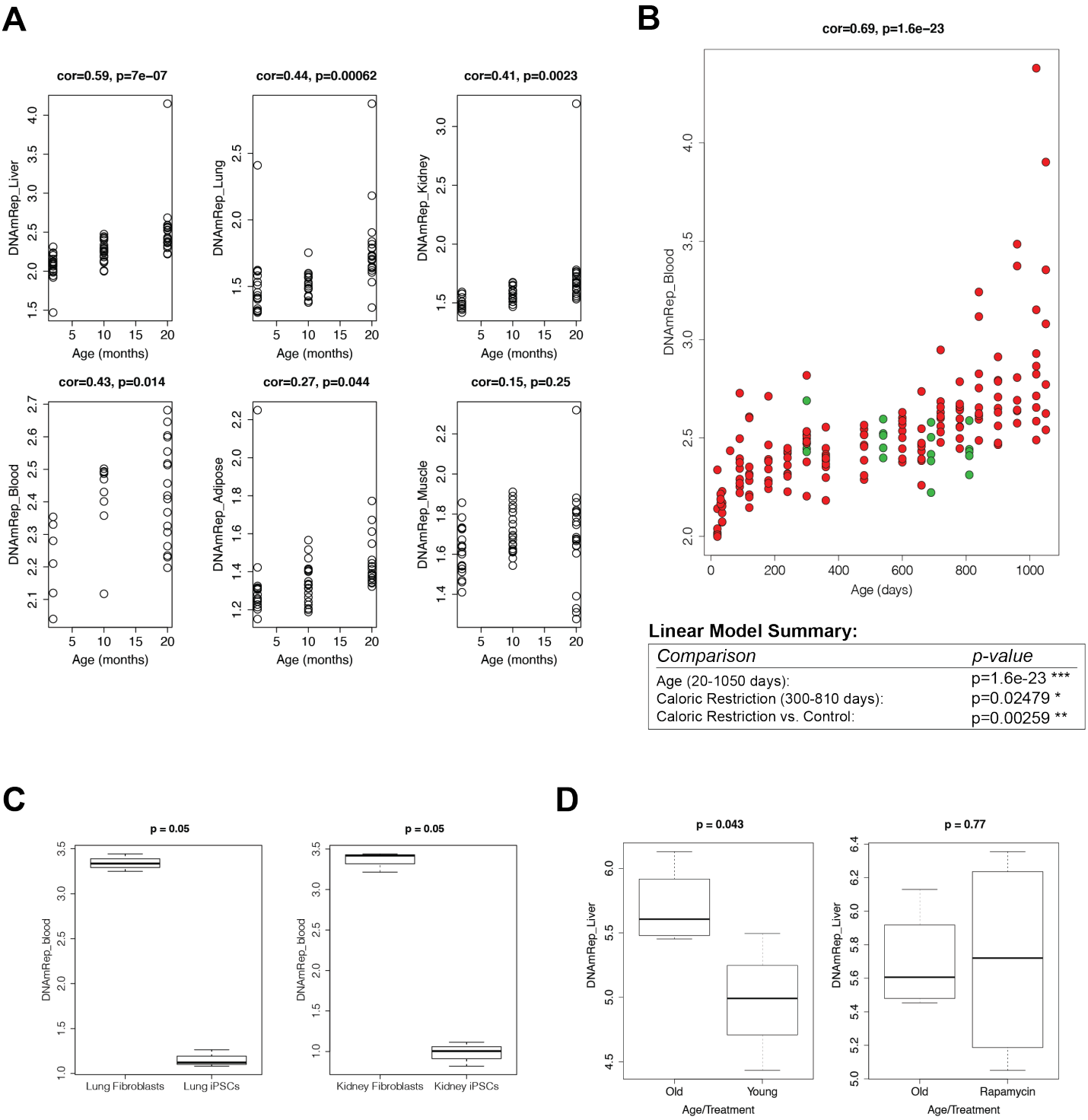

Linear Model Summary:

Comparison	*p-value*
Age (20-1050 days):	p=1.6e-23 ***
Caloric Restriction (300-810 days):	p=0.02479 *
Caloric Restriction vs. Control:	p=0.00259 **

This is a preliminary report of work that has not been certified by peer review.

Figure 3: DNAmRep validates in multiple tissues, including blood and predicts replicative deceleration in caloric restriction and renewal in iPSC reprogrammed cells, but not rapamycin treatment. (A) DNAmRep measure determined in muscle lung, liver, adipose, blood and kidney tissue at 2, 10 and 22 weeks in aged C57BL/6J mice from Thompson et. al 2018. (B) DNAmRep age-association determined from blood data assayed for a non-longitudinal cohort of aged C57BL/6J mice (20-1050 days) in Petkovich et. al 2017. Red samples represent normal chow diet and green samples were calorically restricted (300-810 days), each beginning treatment at 14 weeks. Linear modeling demonstrates statistically significant association by age in normal ($p=1.6e-23$) and CR samples ($p=0.02479$) as well as significant replicative deceleration in CR treated mice ($p=0.00259$). (C) iPSC reprogramming in Lung and Kidney fibroblasts from Petkovich et. al 2017. (D) DNAmRep outcome in liver tissue in Cole et. al 2017 assayed by age (young (2 months) and old (22 month)) and from Rapamycin treatment in C57BL/6J mice.

This is a preliminary report of work that has not been certified by peer review.

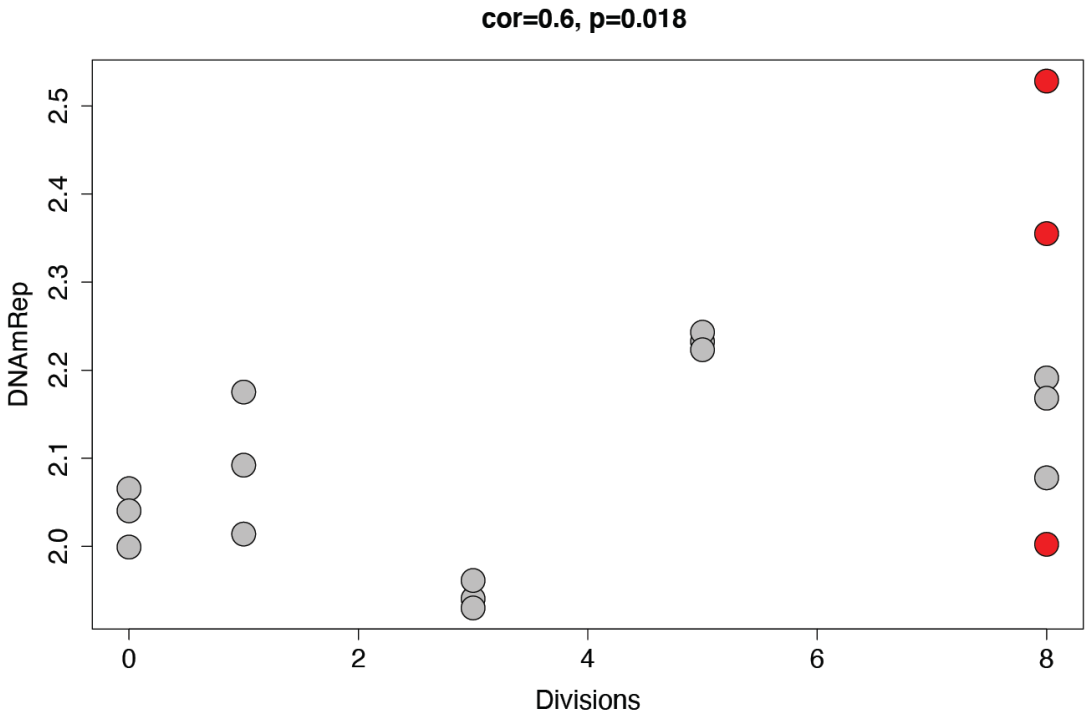

Figure 4: Splenic B cell differentiation demonstrates replicative expansion. DNAmRep measured on 2331 overlapped CpGs in Barwick et. al 2016. Divisions were based on CFSE labeled splenic B220^{+} CD43^{-} cells from naïve C57BL/6J mice that were injected into uMT mice and challenged with LPS after 24h to induce divisions and differentiation. Note, division 8 was further sorted by CD138+ status to confirm terminal differentiation. Grey represents CD138 activity not assayed (Division 0-5) or CD138- (Division 8), where red represents CD138+ populations. Final correlation was determined by removing Division 8 CD138- samples.

This is a preliminary report of work that has not been certified by peer review.

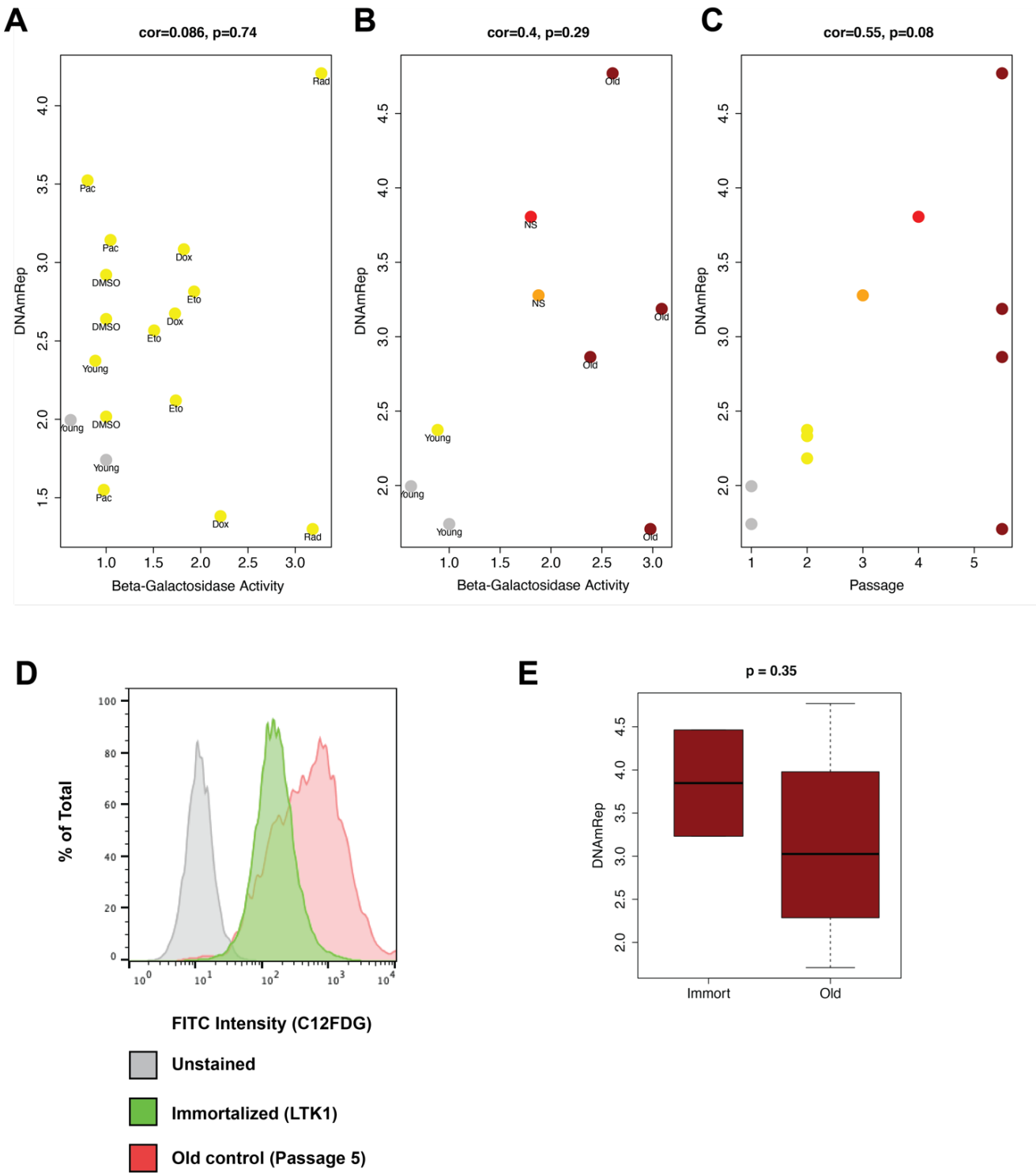

This is a preliminary report of work that has not been certified by peer review.

Figure 5: DNAmRep fails to capture senescence phenotypes independent of cellular passage. (A) DNAmRep measured in irradiation and drug induced senescent samples against DMSO and young (Passage 1) controls. Note, grey=Passage 1, yellow=Passage 2, orange=Passage 3, red=Passage 4 and dark red=Passage 5.5. Pac=Paclitaxel, Dox=Doxyrubicin, Eto=Etoposide and Rad=Irradiation. Senescence induction procedures are outlined in the methods. Beta-Galactosidase activity was determined by FITC fluorescence from C12FDG flow cytometry and normalizing geometric mean with negative samples (unstained) and dividing crude fluorescence by DMSO or young control. (B). DNAmRep score in replicative aged samples organized by Beta-Galactosidase activity. Young=Passage 1-2, NS=Near senescent (Passage 3-4) and Old=Passage 5.5. (C) DNAmRep score in replicative aged sampled organized by passage number. (D) Representative flow cytometry plot demonstrating increased beta-galactosidase activity (FITC intensity) with age compared to immortalized cells. (E) Box plot comparing DNAmRep status between old (passage 5) and old immortalized (passage 5) cells.

This is a preliminary report of work that has not been certified by peer review.

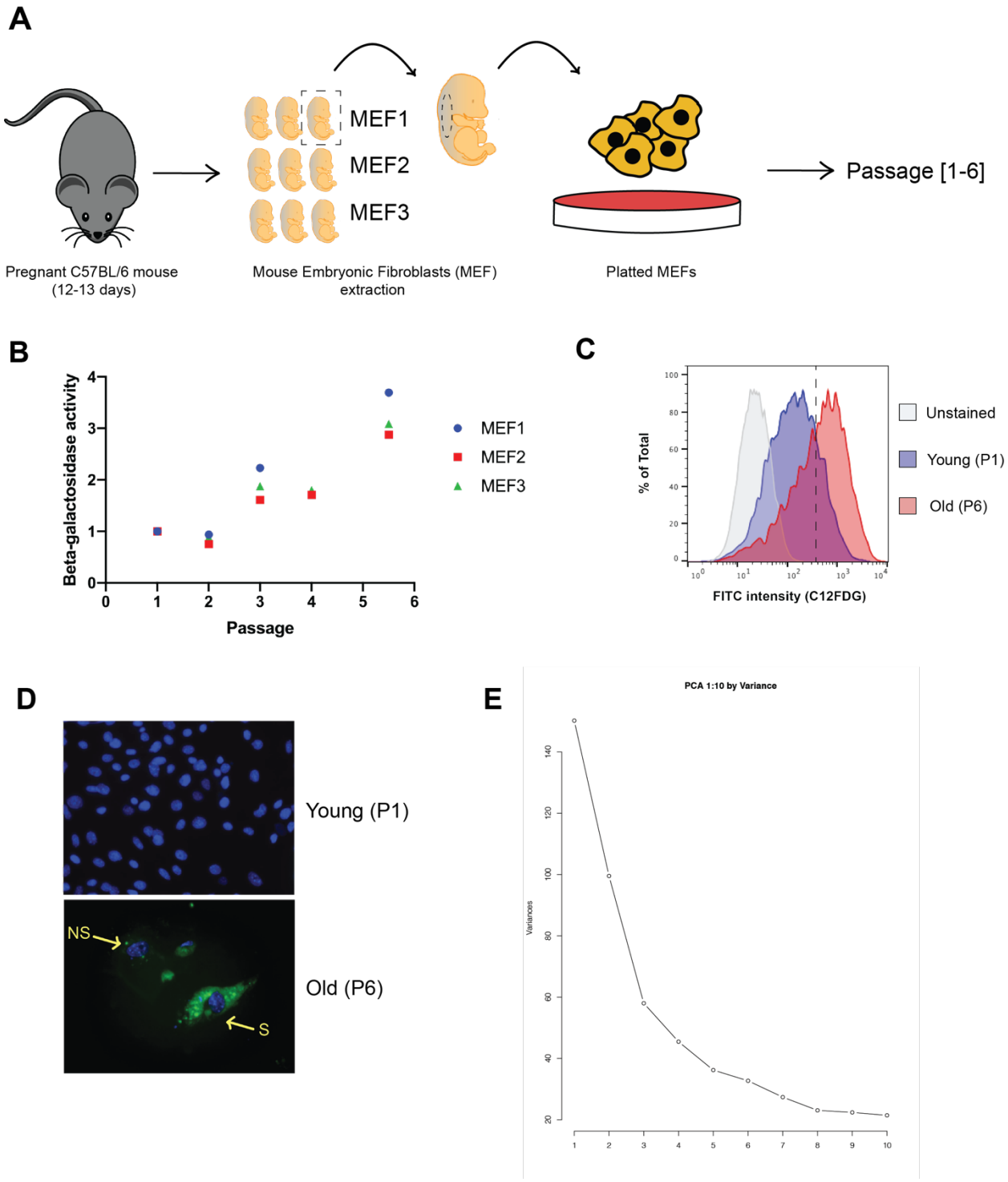

This is a preliminary report of work that has not been certified by peer review.

Supplemental Figure 1: Mouse embryonic fibroblast extraction and passaging. (A) Schematic demonstrating MEF extraction, illustrating embryos were dorsally derived from 12.5-day gestation C57BL/6 mice, then passaged 6x. (B) Flow cytometry plot demonstrating beta-galactosidase activity, as measured by FITC fluorescence from C12FDG probe and normalizing geometric mean with negative samples (unstained) and dividing crude fluorescence by young control (passage 1), is correlated with passage, confirming cells were exhaustively passaged. (C) Representative flow cytometry plot demonstrating older MEFs have greater beta-galactosidase activity. (D) Representative confocal microscopy image (10X) confirming FITC fluorescence from C12FDG is contained to passaged and aged (senescent) cells. S=senescent, NS=Not senescent. (E) Plot measuring PCA components [1-10] from MEF1-3 (passages 1-6) as a function of variance.

This is a preliminary report of work that has not been certified by peer review.

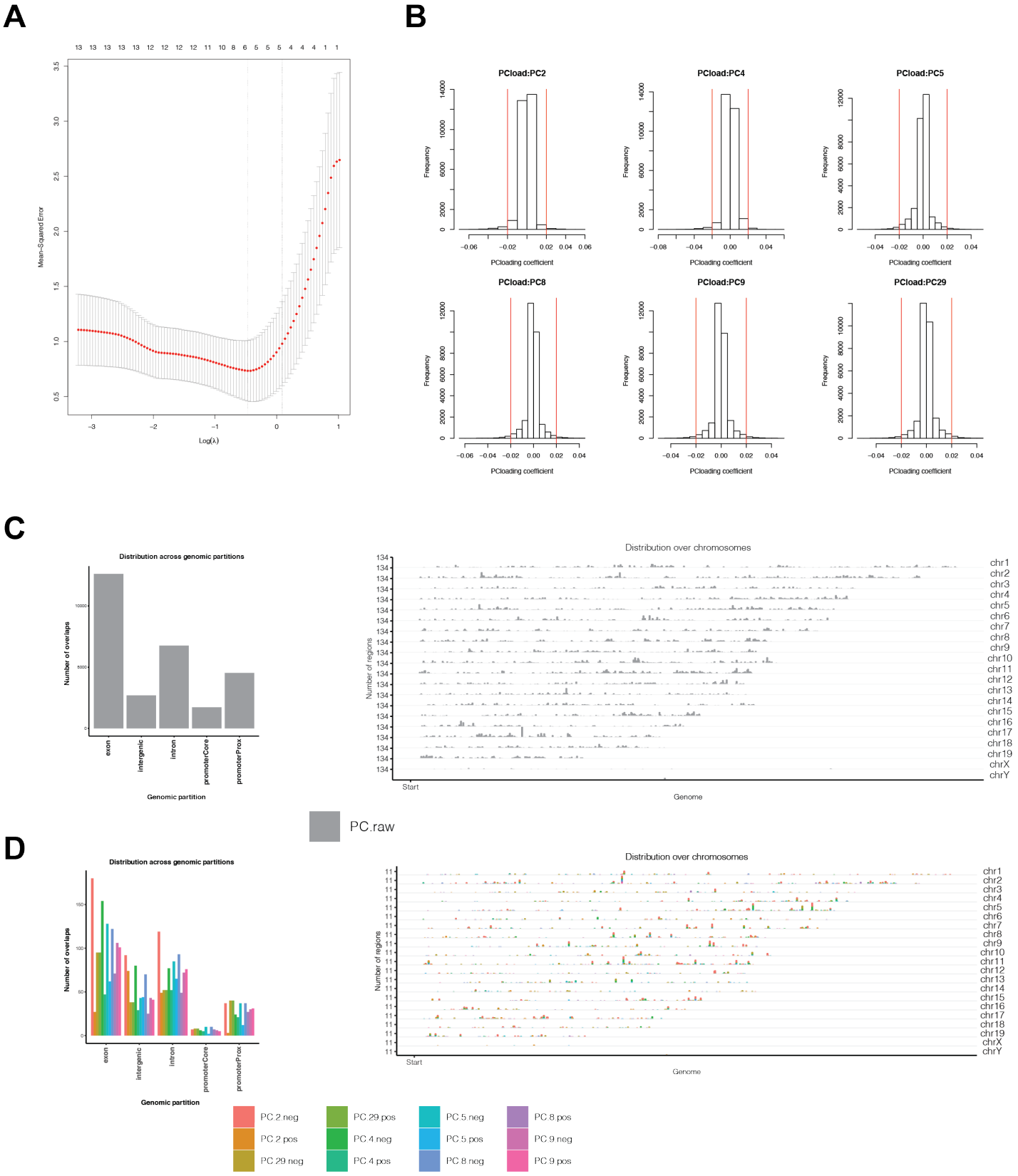

This is a preliminary report of work that has not been certified by peer review.

E

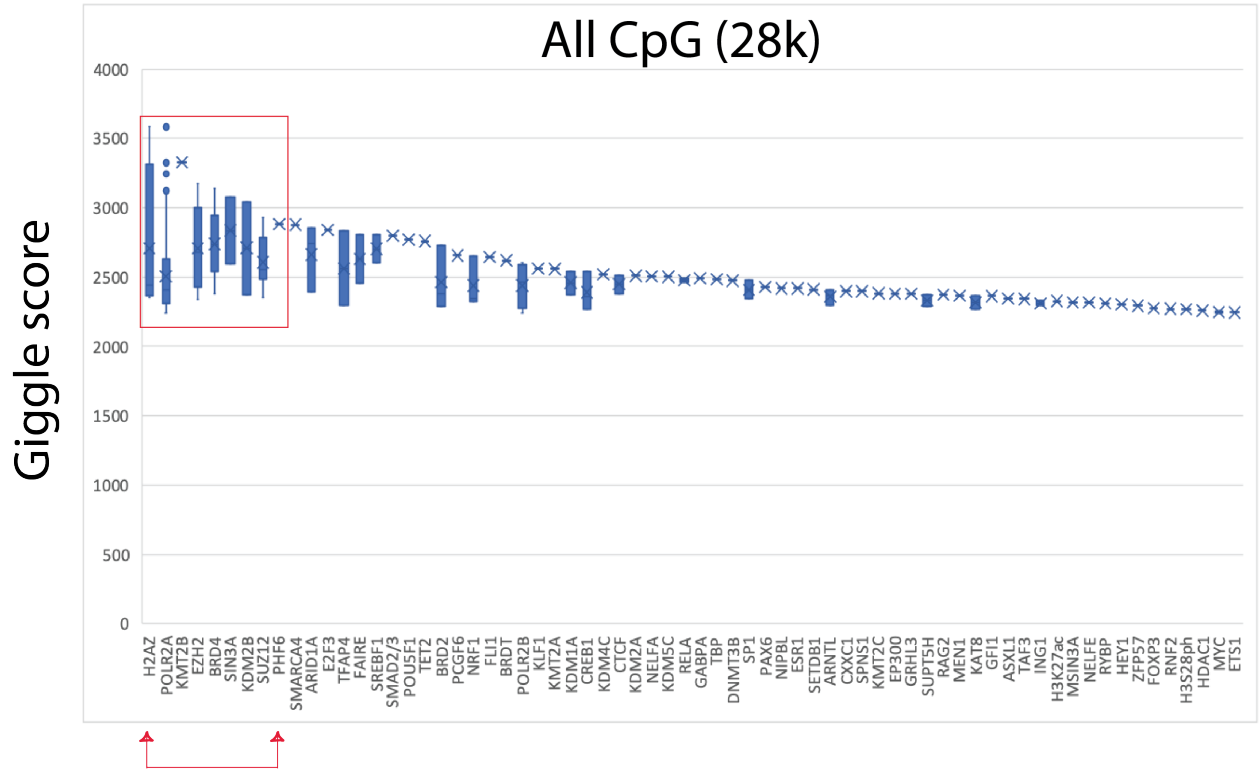

F

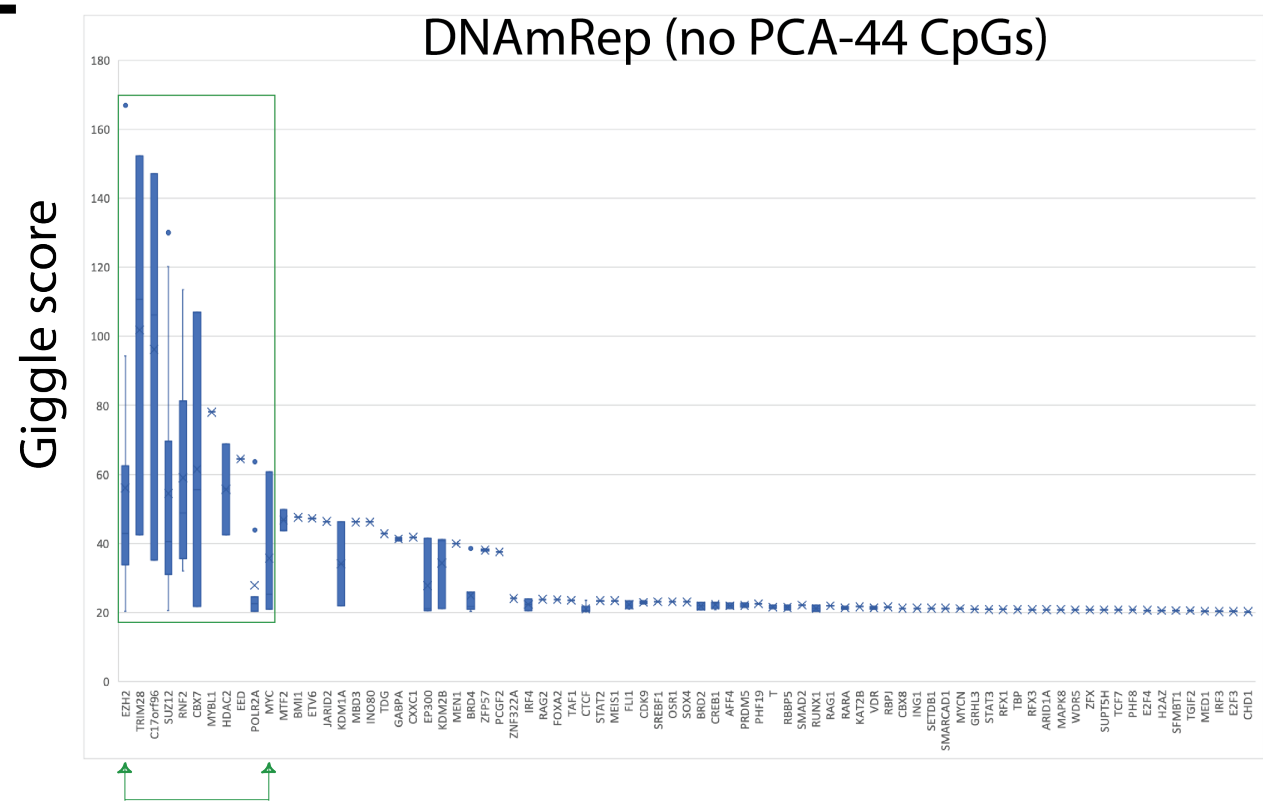

This is a preliminary report of work that has not been certified by peer review.

G

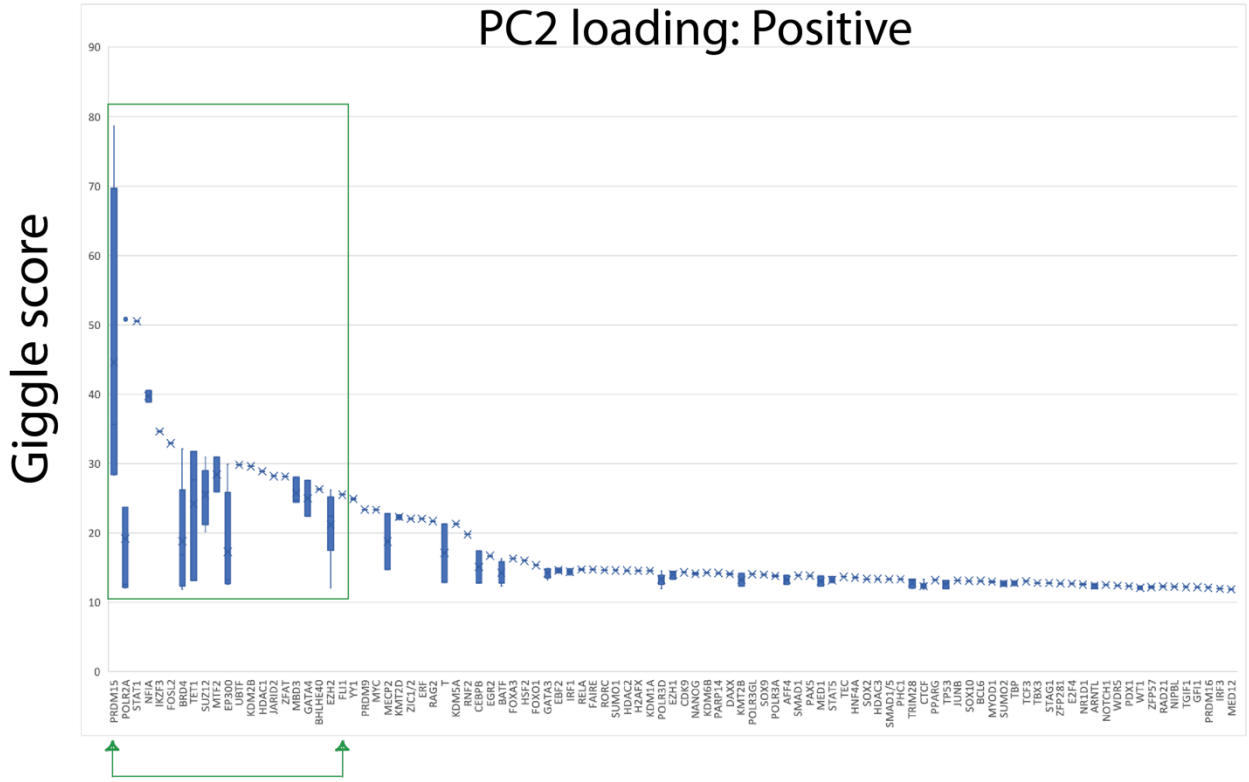

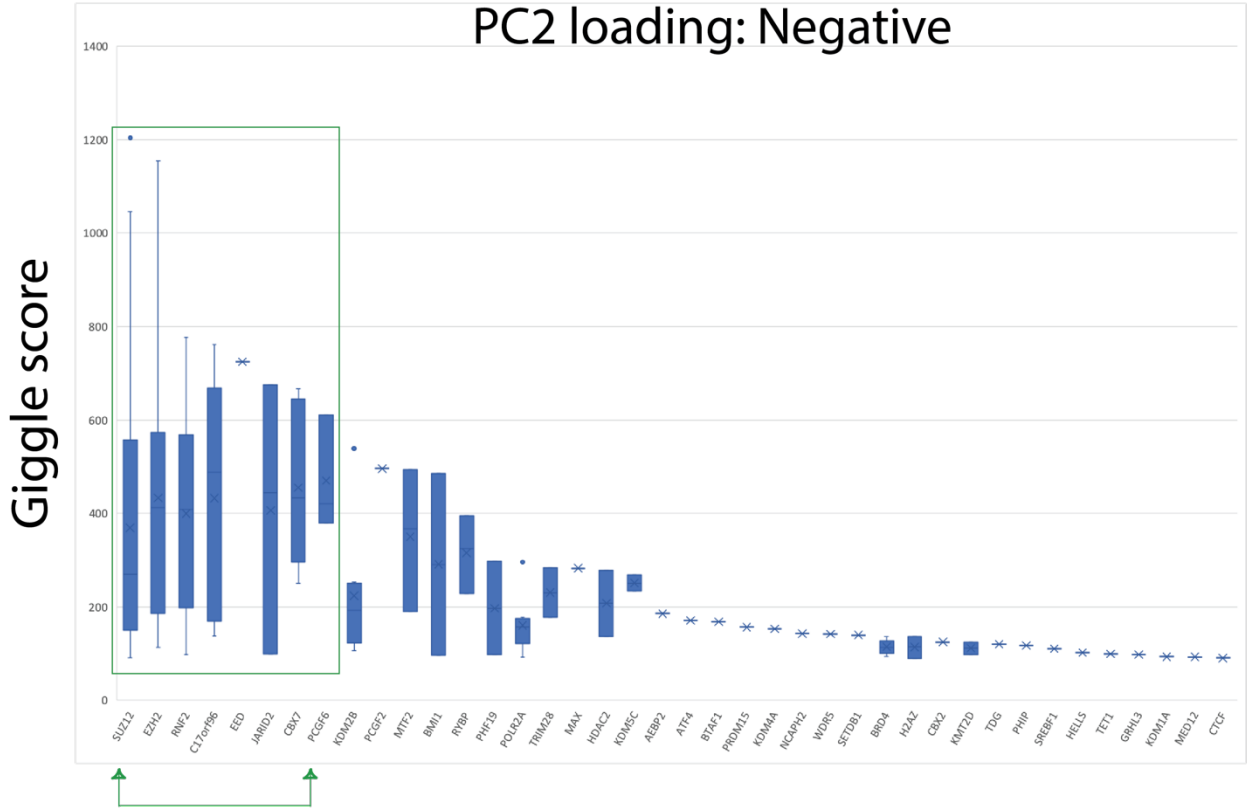

This is a preliminary report of work that has not been certified by peer review.

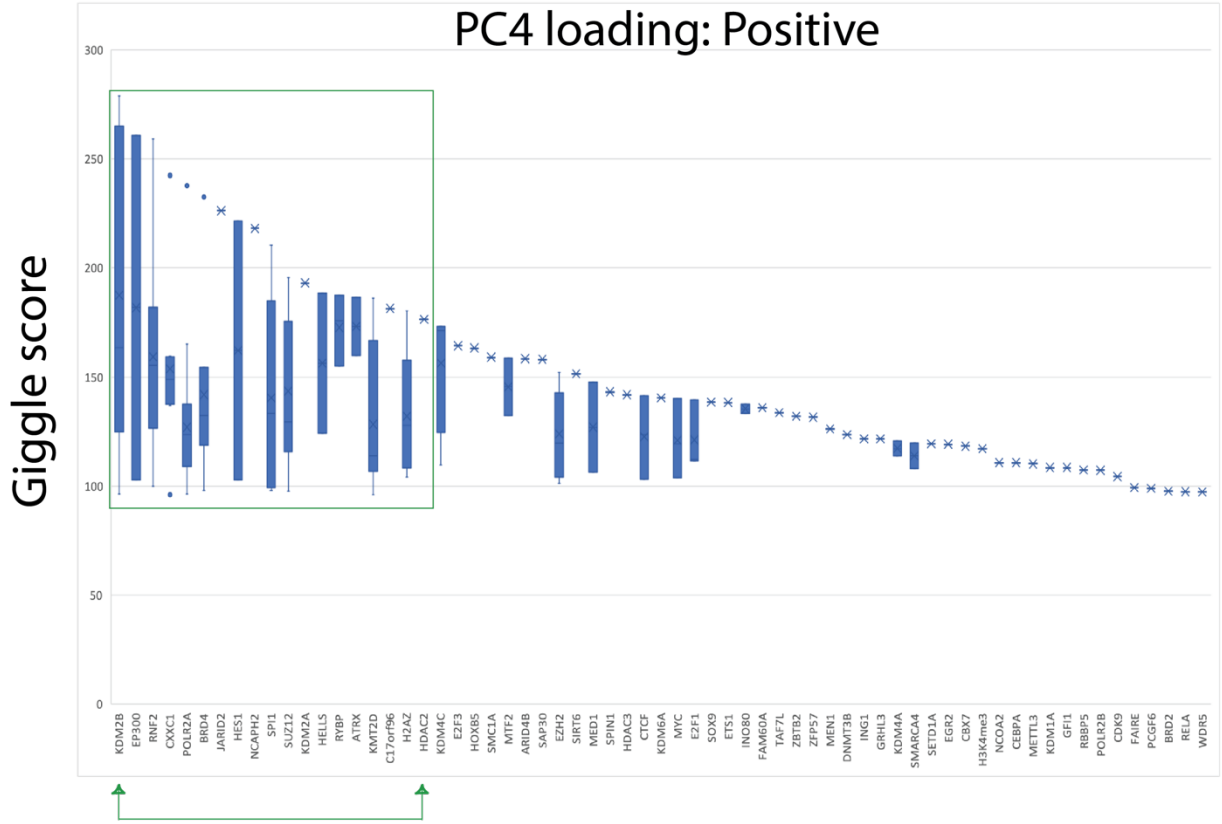

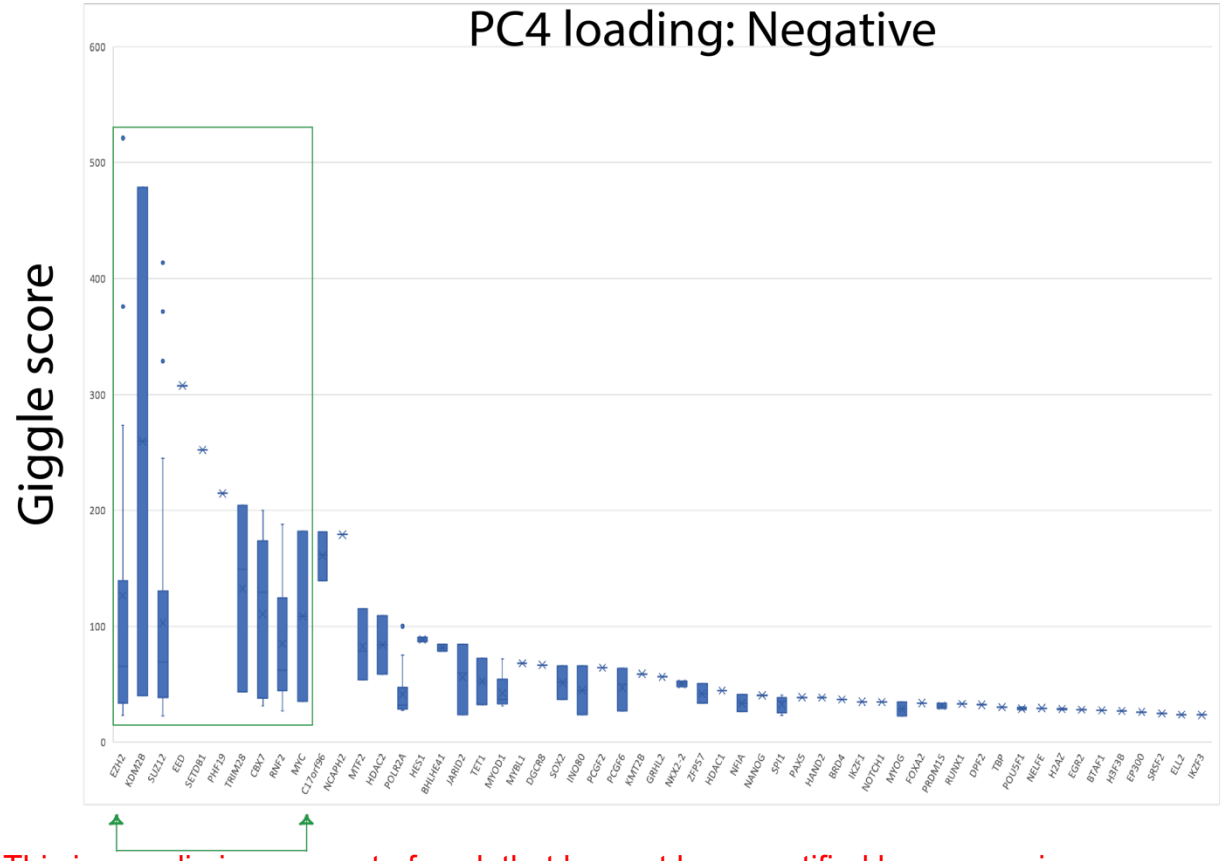

This is a preliminary report of work that has not been certified by peer review.

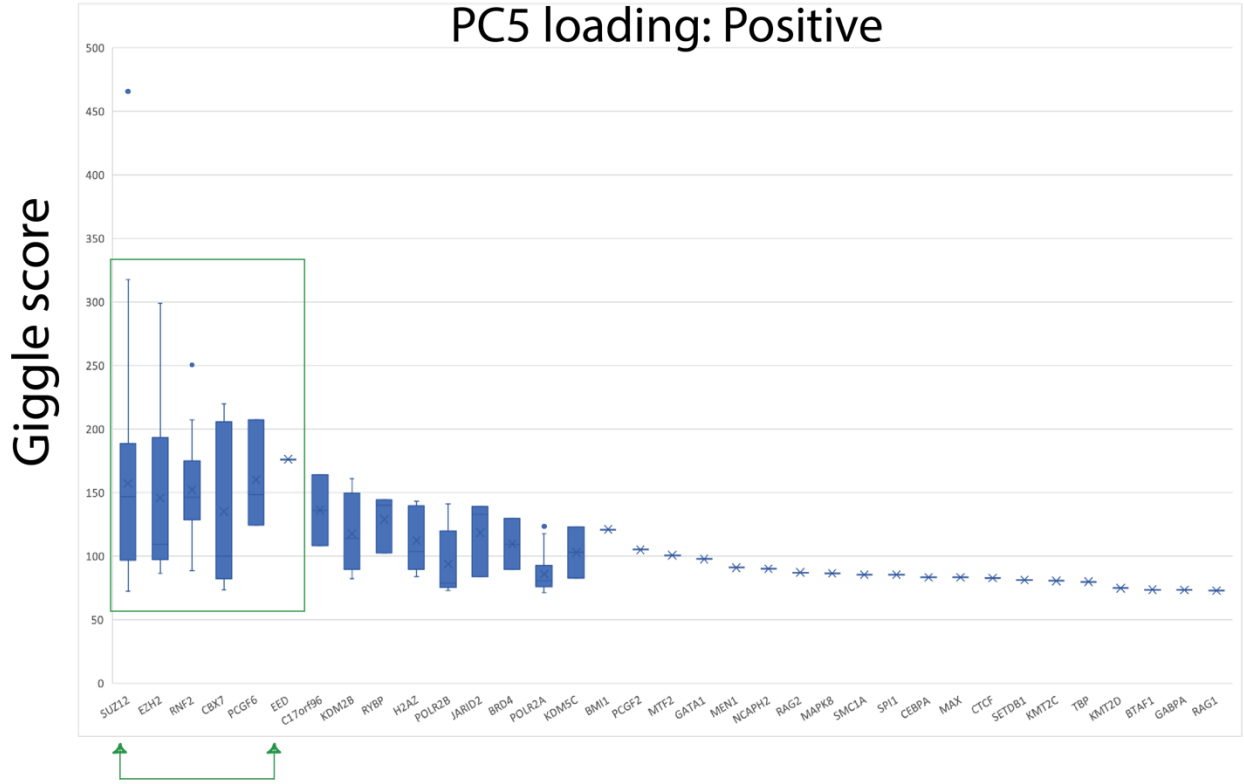

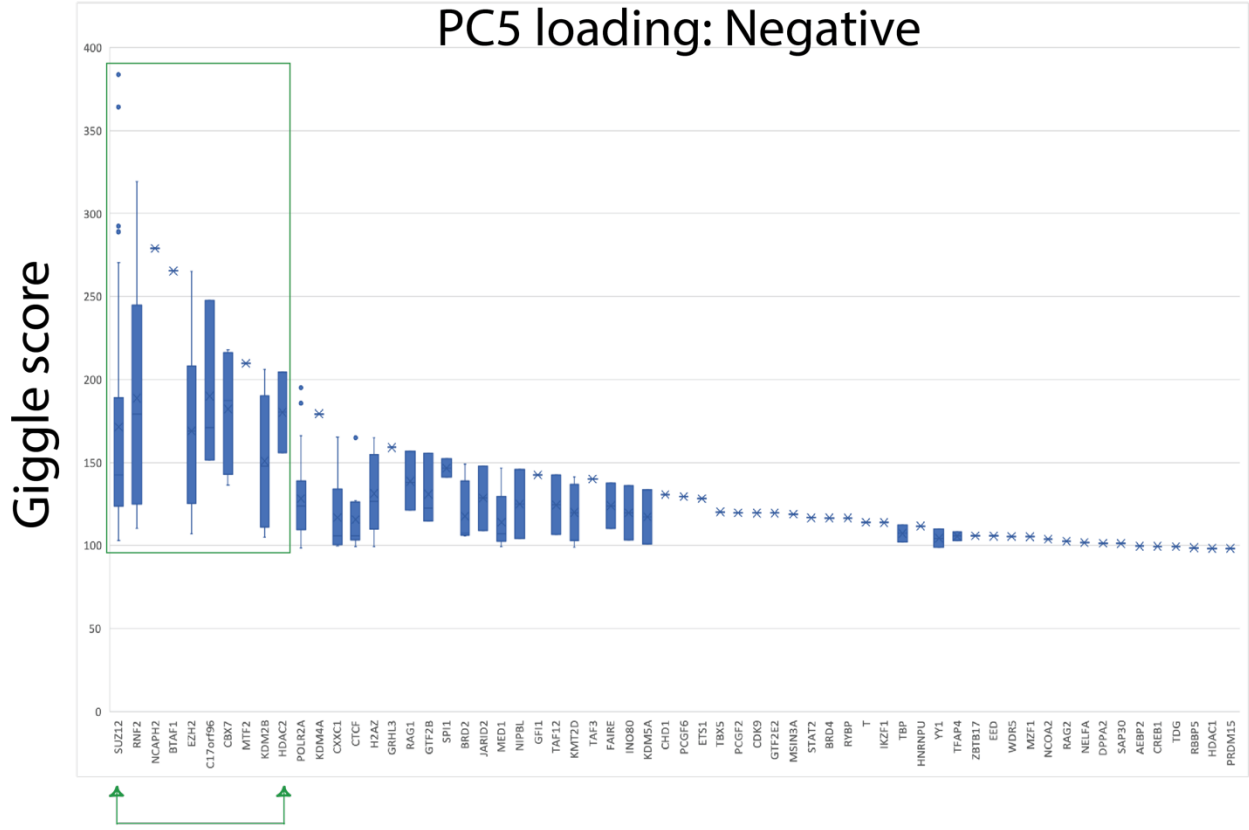

This is a preliminary report of work that has not been certified by peer review.

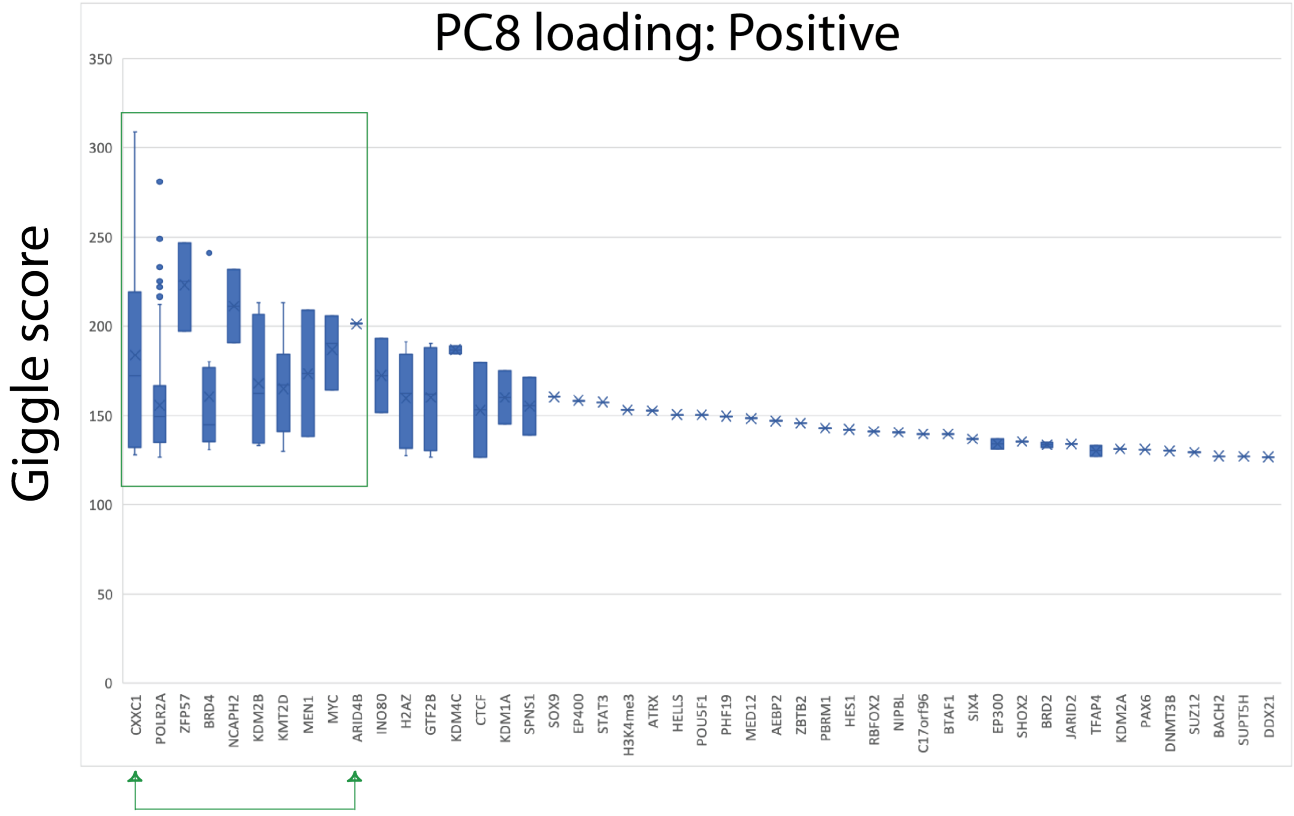

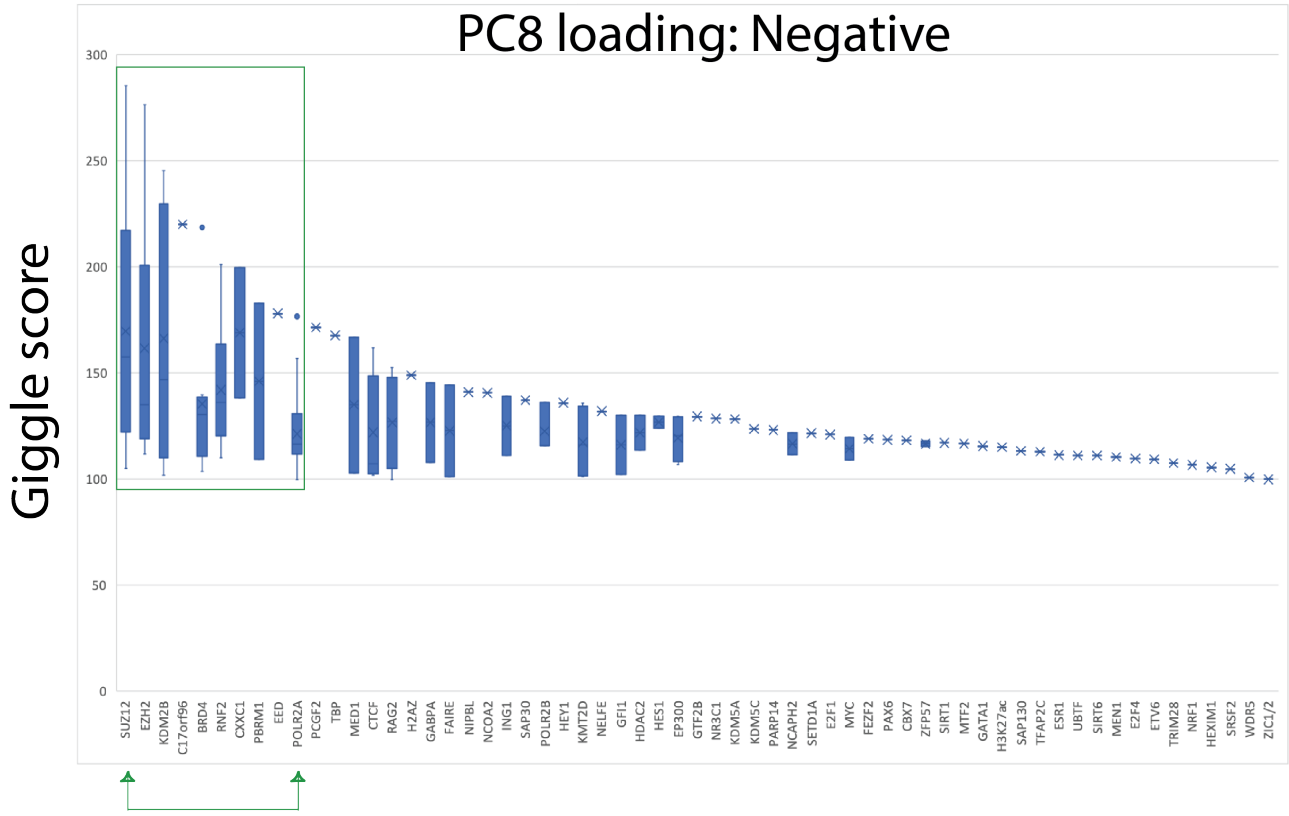

This is a preliminary report of work that has not been certified by peer review.

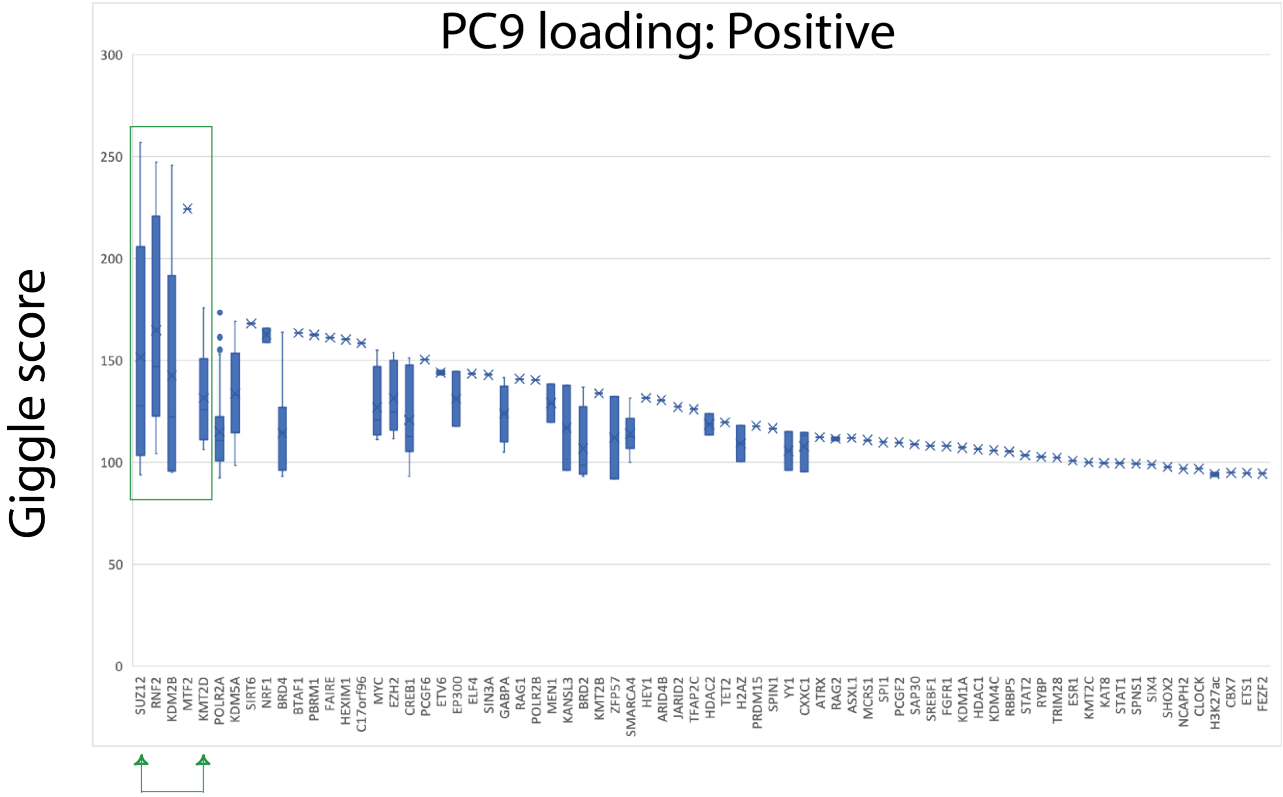

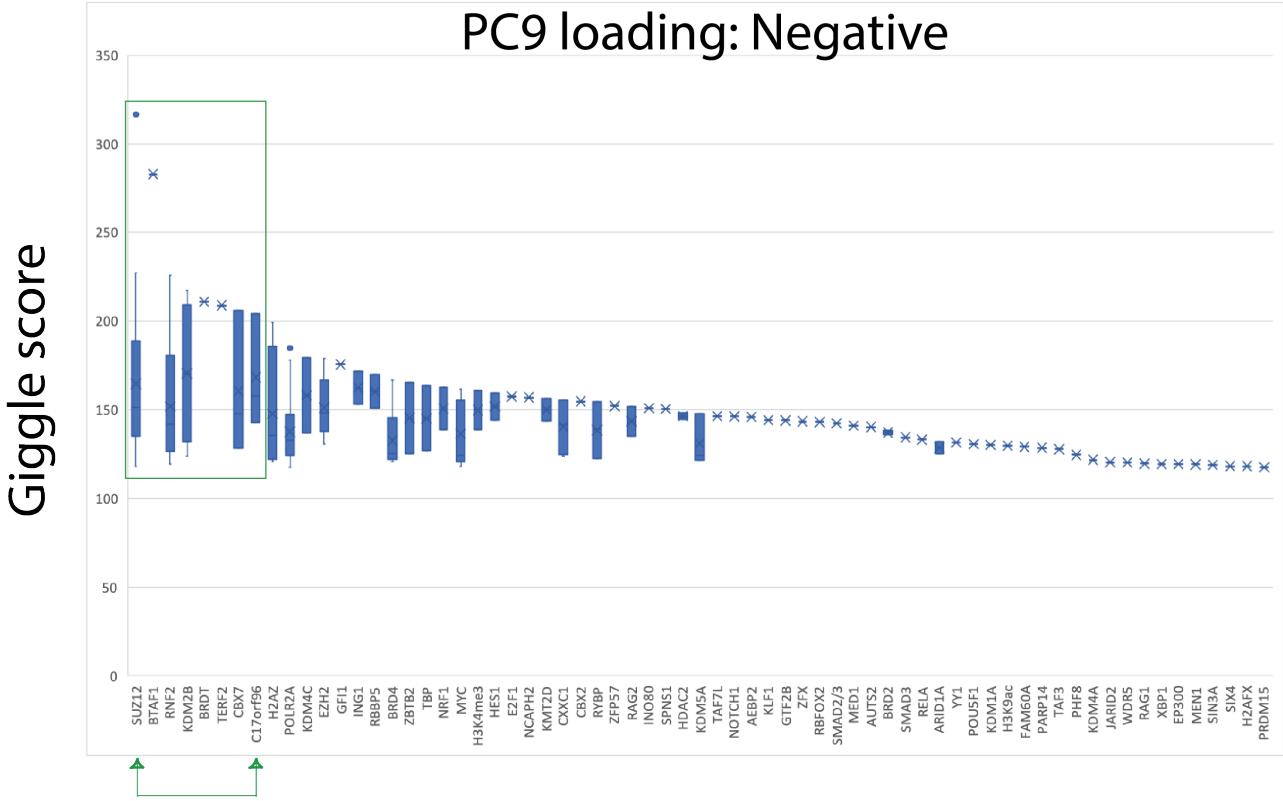

This is a preliminary report of work that has not been certified by peer review.

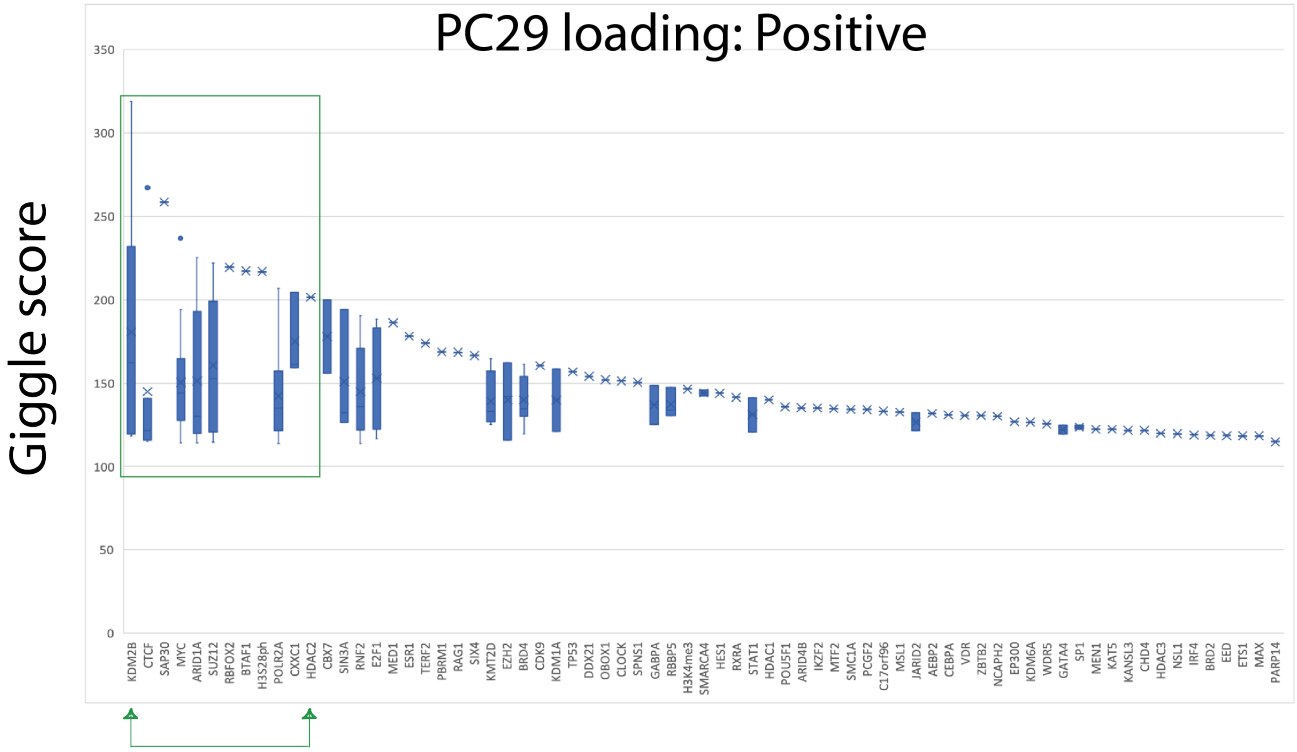

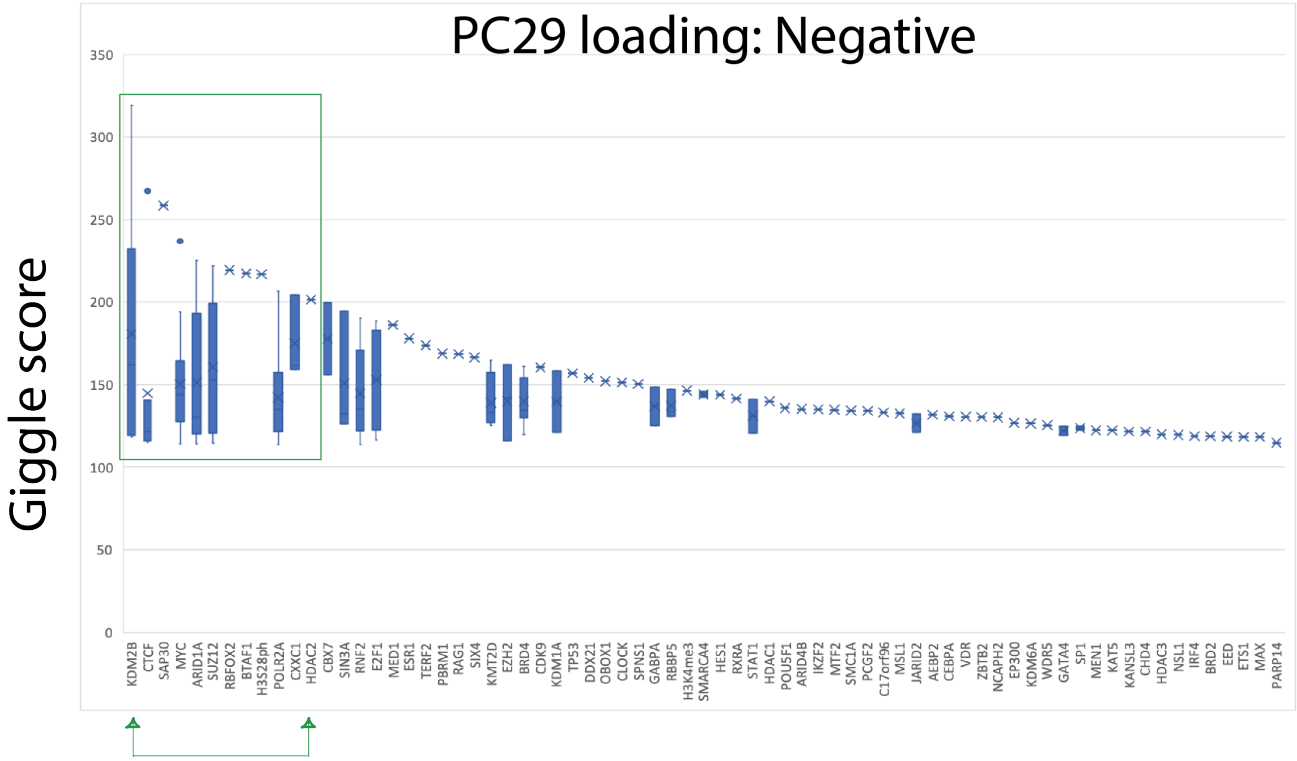

This is a preliminary report of work that has not been certified by peer review.

Supplemental Figure 2: DNAmRep construction, PC loading, CpG distribution and genome enrichment. (A) Elastic net penalized regression plot generating lambda minimum for selecting PCs (PC2, PC4, PC5, PC8, PC9 and PC29) for DNAmRep. (B) Histogram of loaded PCs in DNAmRep, plotted by PC loading coefficient and frequency of total 28,323 CpGs in measure. Red abline represents 0.02 cutoff used to determine CpG drivers of DNAmRep. (C) CpG distribution across chromosomes and genomic partitioning of raw 28,323 CpGs used in DNAmRep, generated by LolaWeb. (D) CpG distribution across chromosomes and genomic partitioning of CpG drivers (N=3087), as determined by 0.02 loading coefficient cutoff. (E-F) Boxplots of enriched genes from Cistrome genome enrichment analysis based on (E) Background 28,323 CpGs, (F) 44 CpGs from DNAmRep trained without PCA and (G) Each PC (>0.02 and <0.02 loading coefficient) from DNAmRep. PC plots were generated after baselining enriched genes to background in (E). Giggle score represents a rank of significance between genomic loci shared between query file and thousands of genome files from databases like ENCODE. We selected the most significant genes in a gene-blinded fashion to not bias overlapped genes. Selected genes are boxed in green, while background genes are boxed in red.

This is a preliminary report of work that has not been certified by peer review.

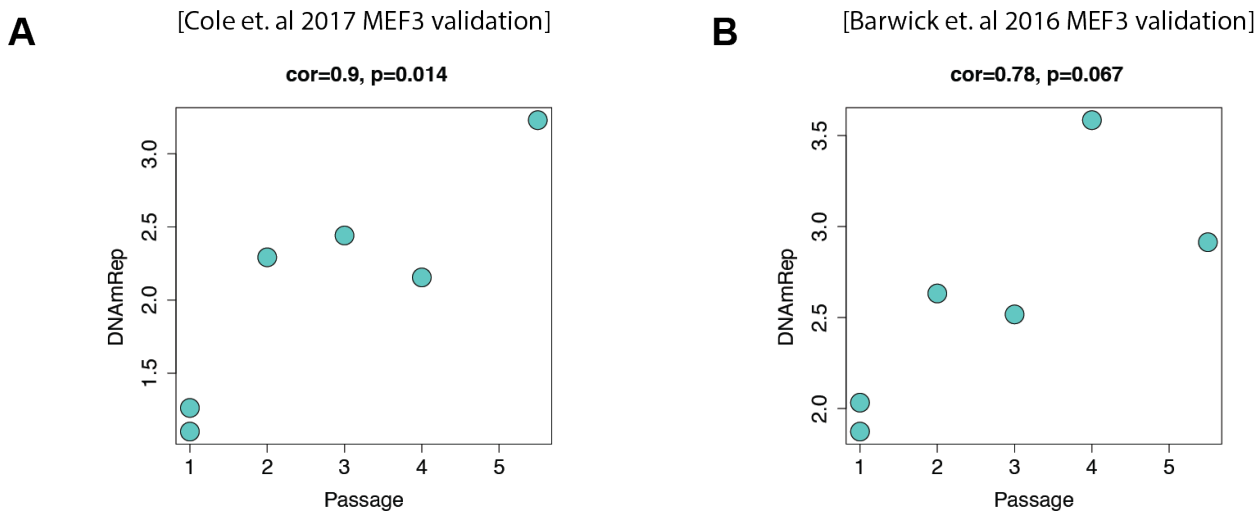

Supplemental Figure 3: MEF3 validation for DNAmRep retraining. (A) MEF3 validation from N=3465 overlapped CpGs with Cole et. al 2017. (B) MEF3 validation from N=2331 overlapped CpGs with Barwick et. al 2016.

This is a preliminary report of work that has not been certified by peer review.

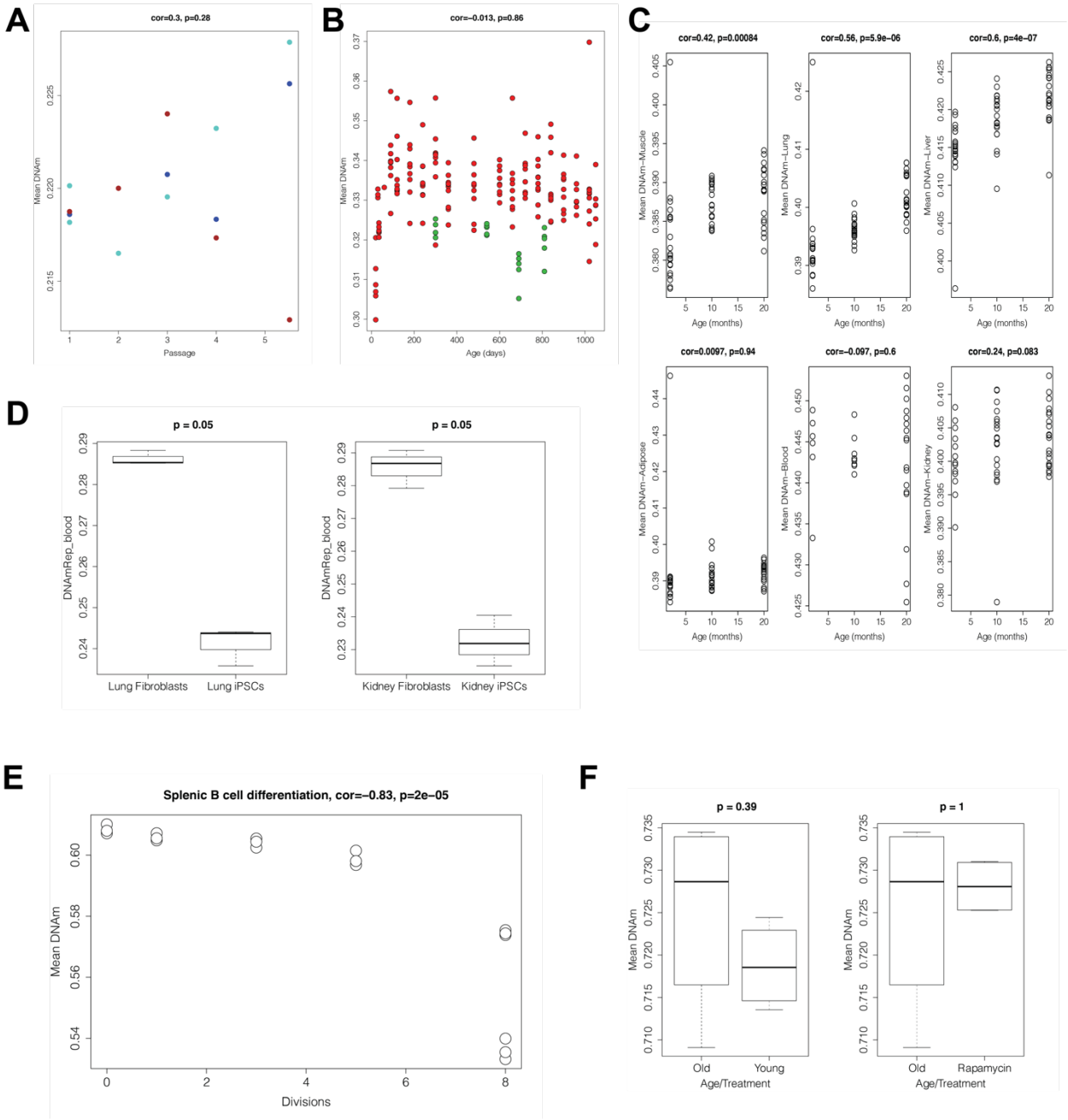

Supplemental Figure 4: Average DNAm in training and validation datasets. Average DNAm in all CpG sites included in analysis from (A) MEF data, (B) Petkovich et. al 2017 aged-blood data (red=normal diet, green=CR), (C) Thompson et. al 2016 tissue data, (D) Petkovich et. al 2017 iPSC data, (E) Barwick et. al 2016 B-cell differentiation data and (F) Cole et. al 2017 liver data.

This is a preliminary report of work that has not been certified by peer review.

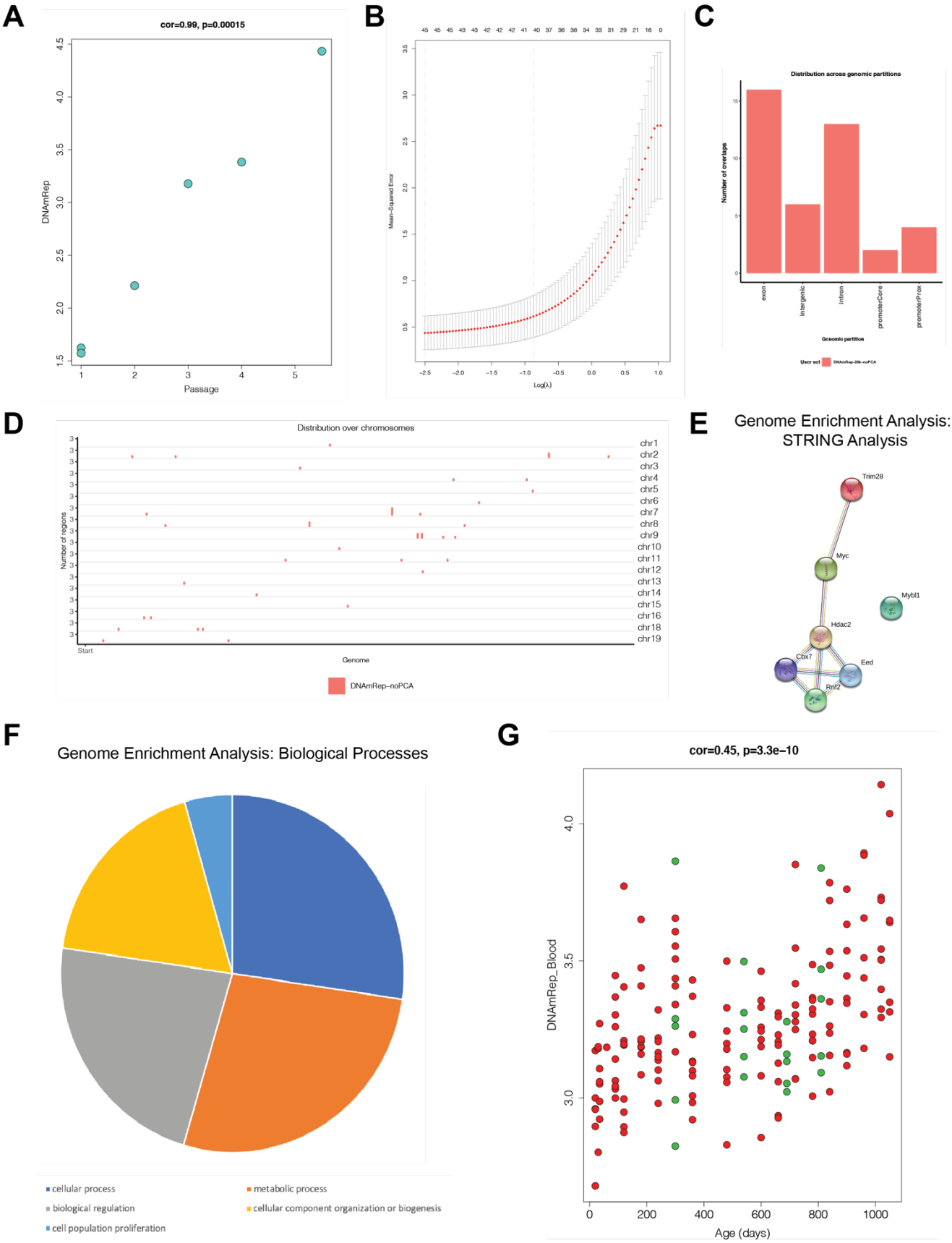

This is a preliminary report of work that has not been certified by peer review.

Supplemental Figure 5: Training a replication predictor using elastic net regression without PCA. As an alternative to DNAmRep, which was trained by conducting elastic net regression on PCA computed samples, we conducted simple elastic net on the bulk 474k CpGs from our original training dataset. (A) 44 CpG DNAmRep score of MEF3 validation trained without PCA. (B) Elastic net penalized regression plot generating lambda minimum for selecting 44 CpGs of interest in no PCA DNAmRep score. (C) Genomic partition and (D) Chromosome distribution of 44 selected CpGs. (E) STRING analysis and (F) Categorized processes of genes selected from genome enrichment analysis in Supplemental Figure 2F. (G) *In vivo* age-validation in Petvokich et. al 2017 blood dataset with normal samples in red and calorie restricted samples in green.

This is a preliminary report of work that has not been certified by peer review.

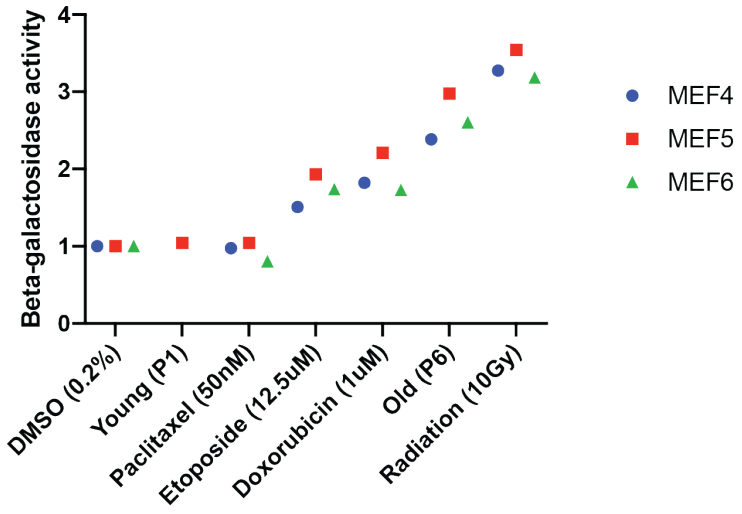

Supplemental Figure 6: Irradiation and drug-induced senescence. Beta-galactosidase activity, as previously reported, measured in MEF4-6 with various damaging and control conditions.

This is a preliminary report of work that has not been certified by peer review.

Methods:

Experimental:

Mouse embryonic fibroblast extraction:

Mouse embryonic fibroblasts (MEFs) were harvested at day 12.5 of gestation. 2 females were used. From the first female, 9 embryos were sacrificed and split into three cell lines, MEF1-3. From the second female, 10 embryos were sacrificed and split into three cell lines, MEF4-6.

Extraction was achieved by separating embryos into separate wells in a 6 well dish using PBS, removing inner embryo and using forceps to carefully remove limbs, head and internal organs from dorsal region. The dorsal region was then cut and trypsinized for 10 minutes at 37°C. To quench reaction cells were transferred to a 15 mL falcon tube and spun for 3 minutes at 1200 rpm, then supernatant was aspirated and resuspended with 10 mL DMEM. P0 cells were split once to expand cell number prior to freezing. Approximately 2 mL of cells were incubated overnight with 8 mL DMEM and following growth were tryponsized and either passaged for experiments or stored at -80°C in DMEM/DMSO (90:10).

Replicative passaging and cell culture:

Cells were split/passaged 6 times, where flow cytometry/confocal microscopy and RRBS sequencing were conducted at each passage.

Cells were split according to the starting seeding density below and were counted using Invitrogen countess and cell counting chamber slide with trypan blue. For media, we used DMEM + 10% FBS + 1% PENSTREP. Note, later passaged cells had a lower platting efficiency when inspected visually 24 hours after seeding and we used a cell scraper prior to transfer otherwise senescent cells remained attached to the dish. Cells were split at approximately 95% confluence which occurred around 3-4 days in P1-3 and 5-8 days in P4-6.

p100 - 0.5×10^6 cells
p60 - 0.25×10^6 cells
6 well - 0.125×10^6 cells

Plasmid transfection:

LTK1 (Immortalization) and empty vector (pBABE) plasmids were described previously [69]. Briefly, Phoenix Amphotropic cells were used to grow virus as described previously [70,71] and puromycin (0.5 µg/µl) and blasticidin (2 µg/µl) were used for selection.

Beta-galactosidase flow cytometry and confocal microscopy:

This is a preliminary report of work that has not been certified by peer review.

To conduct beta-galactosidase flow cytometry, approximately $0.25x10^6$ cells were seeded into p60 dishes and pre-treatment was conducted approximately 16 hours after seeding. Cells were first pre-treated with Bafilomycin A1 (Selleckchem: S1413, 622.83 g/mol, 100 μM stock). Existing DMEM was aspirated, then cells were washed with PBS and replaced with treated Bafilomycin A1 DMEM for 30 minutes at a final concentration of 100 nM. Following Bafilomycin A1 pre-treatment to normalize lysosome activity, C12FDG (Invitrogen: D2893, 853.92 g/mol, 10 mM stock) was added directly to the existing media for 90 minutes at a final concentration of 20 μM. Note, due to light sensitivity, exchange was conducted in a dark environment.

For determining beta-galactosidase activity via flow cytometry, treated cells were trypsinized (1 mL-p60) for 5 minutes at 37°C and then quenched using 3 mL DMEM. Note, cells were completely detached using a cell scraper prior to transfer otherwise senescent cells remained attached to the dish. After thorough resuspension, cells were transferred directly to a filter top tube and spun for 3 minutes at 1200 rpm. Supernatant was aspirated and cells were resuspended in 100 μL PBS and immediately assayed using a 488 nM laser on a StratedigmS1000 benchtop flow cytometer. Fluorescence intensity was normalized and baselined using an unstained sample. FlowJo (10.6.1) was used to analyze data and beta-galactose activity/senescence activity was determined as FITC treated geometric mean/control geometric mean.

For determining beta-galactosidase activity via confocal microscopy, cells were split into 12 well dishes with a glass cover slide at the bottom of each well. Following Bafilomycin A1 and C12FDG treatment, media was aspirated and cells were washed with PSB 3x, fixed with 4% PFA/PBS (10 minutes), followed by 2x PSB washes and then counter stained with DAPI and mounted onto cover slips. Fixed cells were immediately imaged at 4x, 10x and 40x resolution using a Keyence confocal cytometer.

Senescence induction:

We induced senescence using previously established conditions [46,47]. In brief, MEFs were thawed and allow to expand for one passage, then split to a normalized seeding density of $0.25x10^6$ cell/p60 and $0.125x10^6$ cells/6-well and treatment was conducted for 5 days. Note, senescence induction experiments were conducted at passage 2. Doxyrubicin (Sigma: D1515, 1 μM), Paclitaxel (Sigma: T7402, 50 nM) and Etoposide (Sigma: E1383, 12.5 μM) were all dosed into DMEM when the cells were split and media was not replaced for the duration of the 5-day treatment. We irradiated cells (10 Gy) using cesium irradiation and collected these cells after 5 days as well.

DNA preparation and quantification:

DNA was extracted from selected samples prior to RRBS sequencing using a Qiagen DNeasy Blood and Tissue extraction kit (69504). Note, samples were treated with proteinase K and RNAse A and eluted with 200 μl elution buffer. Following final elution, DNA was verified using nanodrop (Thermo Scientific). Spin concentration was used as necessary with low DNA content samples. Prior to library preparation we used a qubit

This is a preliminary report of work that has not been certified by peer review.

fluorometer (Thermo Scientific) to quantify the extracted genomic DNA. All samples were assigned a single-blinded code and randomized for library preparation and sequencing to control for any batch errors.

Library preparation and *reduced representation bisulfide sequencing:*

Library preparation was conducted using EZ DNA Methylation RRBS Library Prep Kit (Zymo: D5461), according to manufacturer's recommendations. Randomized and pooled samples were sequenced on four Illumina NovaSeq6000 SP lanes (100 bases single-end mode). Note, each lane produced more than 400M reads.

Computational:
Data clean up and CpG selection:

FastQC (v0.11.8) was used to assess the quality of the raw reads and adapter-trimmed reads (cutadapt, version 2.5). Reads were mapped to the GRCm38 RRBS genome using BSBolt v0.1.2 (https://github.com/NuttyLogic/BSBolt). Methylation was called and the CpG methylation matrix was assembled for CpG sites common to all samples and covered by more than 10 reads. The final matrix consisted of 474,128 CpG sites.

Statistical Analysis:

R was the primary platform used for statistical analysis. For determining statistical significance, the Fisher test was used for two groups and the Kruskal Wallis test (non-parametric) was used for multiple groups. We used elastic net penalized regression (glmnet) to train all predictors and also integrated principal component analysis into the final DNAmRep model. Genome enrichment analysis was conducted using Cistrome, genomic partitioning and CpG locations were determined using LolaWeb and Panther was used to group enriched genes by biological process and function.

This is a preliminary report of work that has not been certified by peer review.

References:

(1) Campisi, J., Kapahi, P., Lithgow, G.J., Melov, S., Newman, J.C. and Verdin, E., 2019. From discoveries in ageing research to therapeutics for healthy ageing. *Nature*, *571*(7764), pp.183-192.
(2) Larsson, S.C., Kaluza, J. and Wolk, A., 2017. Combined impact of healthy lifestyle factors on lifespan: two prospective cohorts. *Journal of internal medicine*, *282*(3), pp.209-219.
(3) Blasco, M.A., 2007. Telomere length, stem cells and aging. *Nature chemical biology*, *3*(10), pp.640-649.
(4) Xu, M., Pirtskhalava, T., Farr, J.N., Weigand, B.M., Palmer, A.K., Weivoda, M.M., Inman, C.L., Ogrodnik, M.B., Hachfeld, C.M., Fraser, D.G. and Onken, J.L., 2018. Senolytics improve physical function and increase lifespan in old age. *Nature medicine*, *24*(8), pp.1246-1256.
(5) Tchkonia, T., Morbeck, D.E., Von Zglinicki, T., Van Deursen, J., Lustgarten, J., Scrable, H., Khosla, S., Jensen, M.D. and Kirkland, J.L., 2010. Fat tissue, aging, and cellular senescence. *Aging cell*, *9*(5), pp.667-684.
(6) Tchkonia, T., Zhu, Y., Van Deursen, J., Campisi, J. and Kirkland, J.L., 2013. Cellular senescence and the senescent secretory phenotype: therapeutic opportunities. *The Journal of clinical investigation*, *123*(3), pp.966-972.
(7) Hoeijmakers, J.H., 2009. DNA damage, aging, and cancer. *New England Journal of Medicine*, *361*(15), pp.1475-1485.
(8) Oh, J., Lee, Y.D. and Wagers, A.J., 2014. Stem cell aging: mechanisms, regulators and therapeutic opportunities. *Nature medicine*, *20*(8), pp.870-880.
(9) Zhang, Y., Wilson, R., Heiss, J., Breitling, L.P., Saum, K.U., Schöttker, B., Holleczek, B., Waldenberger, M., Peters, A. and Brenner, H., 2017. DNA methylation signatures in peripheral blood strongly predict all-cause mortality. *Nature communications*, *8*(1), pp.1-11.
(10) Izzo, F., Lee, S.C., Poran, A., Chaligne, R., Gaiti, F., Gross, B., Murali, R.R., Deochand, S.D., Ang, C., Jones, P.W. and Nam, A.S., 2020. DNA methylation disruption reshapes the hematopoietic differentiation landscape. *Nature Genetics*, *52*(4), pp.378-387.
(11) Ferry, L., Fournier, A., Tsusaka, T., Adelmant, G., Shimazu, T., Matano, S., Kirsh, O., Amouroux, R., Dohmae, N., Suzuki, T. and Filion, G.J., 2017. Methylation of DNA ligase 1 by G9a/GLP recruits UHRF1 to replicating DNA and regulates DNA methylation. *Molecular cell*, *67*(4), pp.550-565.
(12) Riggs, A.D., 1975. X inactivation, differentiation, and DNA methylation. *Cytogenetic and Genome Research*, *14*(1), pp.9-25.
(13) Murgatroyd, C., Patchev, A.V., Wu, Y., Micale, V., Bockmühl, Y., Fischer, D., Holsboer, F., Wotjak, C.T., Almeida, O.F. and Spengler, D., 2009. Dynamic DNA methylation programs persistent adverse effects of early-life stress. *Nature neuroscience*, *12*(12), pp.1559-1566.
(14) Li, E., Beard, C. and Jaenisch, R., 1993. Role for DNA methylation in genomic imprinting. *Nature*, *366*(6453), pp.362-365.
(15) Hata, K., Okano, M., Lei, H. and Li, E., 2002. Dnmt3L cooperates with the Dnmt3 family of de novo DNA methyltransferases to establish maternal imprints in mice. *Development*, *129*(8), pp.1983-1993.
(16) Chedin, F., 2011. The DNMT3 family of mammalian de novo DNA methyltransferases. In *Progress in molecular biology and translational science* (Vol. 101, pp. 255-285). Academic Press.
(17) Fuks, F., Burgers, W.A., Brehm, A., Hughes-Davies, L. and Kouzarides, T., 2000. DNA methyltransferase Dnmt1 associates with histone deacetylase activity. *Nature genetics*, *24*(1), pp.88-91.
(18) Rhee, I., Bachman, K.E., Park, B.H., Jair, K.W., Yen, R.W.C., Schuebel, K.E., Cui, H., Feinberg, A.P., Lengauer, C., Kinzler, K.W. and Baylin, S.B., 2002. DNMT1 and DNMT3b cooperate to silence genes in human cancer cells. *Nature*, *416*(6880), pp.552-556.
(19) Zöchbauer-Müller, S., Fong, K.M., Virmani, A.K., Geradts, J., Gazdar, A.F. and Minna, J.D., 2001. Aberrant promoter methylation of multiple genes in non-small cell lung cancers. *Cancer research*, *61*(1), pp.249-255.
(20) Shen, L., Kondo, Y., Rosner, G.L., Xiao, L., Hernandez, N.S., Vilaythong, J., Houlihan, P.S., Krouse, R.S., Prasad, A.R., Einspahr, J.G. and Buckmeier, J., 2005. MGMT promoter methylation

This is a preliminary report of work that has not been certified by peer review.

and field defect in sporadic colorectal cancer. *Journal of the National Cancer Institute*, *97*(18), pp.1330-1338.
(21)Mette, M.F., Aufsatz, W., Van der Winden, J., Matzke, M.A. and Matzke, A.J.M., 2000. Transcriptional silencing and promoter methylation triggered by double-stranded RNA. *The EMBO journal*, *19*(19), pp.5194-5201.
(22)Aran, D., Sabato, S. and Hellman, A., 2013. DNA methylation of distal regulatory sites characterizes dysregulation of cancer genes. *Genome biology*, *14*(3), pp.1-14.
(23)Deng, G., Kakar, S., Tanaka, H., Matsuzaki, K., Miura, S., Sleisenger, M.H. and Kim, Y.S., 2008. Proximal and distal colorectal cancers show distinct gene-specific methylation profiles and clinical and molecular characteristics. *European journal of cancer*, *44*(9), pp.1290-1301.
(24)Mays-Hoopes, L.L., 1989. Age-related changes in DNA methylation: do they represent continued developmental changes?. In *International review of cytology* (Vol. 114, pp. 181-220). Academic Press.
(25)Ahuja, N. and Issa, J.P., 2000. Aging, methylation and cancer.
(26)Levine, M.E., Lu, A.T., Quach, A., Chen, B.H., Assimes, T.L., Bandinelli, S., Hou, L., Baccarelli, A.A., Stewart, J.D., Li, Y. and Whitsel, E.A., 2018. An epigenetic biomarker of aging for lifespan and healthspan. *Aging (Albany NY)*, *10*(4), p.573.
(27)Lu, A.T., Quach, A., Wilson, J.G., Reiner, A.P., Aviv, A., Raj, K., Hou, L., Baccarelli, A.A., Li, Y., Stewart, J.D. and Whitsel, E.A., 2019. DNA methylation GrimAge strongly predicts lifespan and healthspan. *Aging (Albany NY)*, *11*(2), p.303.
(28)Hannum, G., Guinney, J., Zhao, L., Zhang, L., Hughes, G., Sadda, S., Klotzle, B., Bibikova, M., Fan, J.B., Gao, Y. and Deconde, R., 2013. Genome-wide methylation profiles reveal quantitative views of human aging rates. *Molecular cell*, *49*(2), pp.359-367.
(29)Horvath, S., 2013. DNA methylation age of human tissues and cell types. *Genome biology*, *14*(10), p.3156.
(30)Horvath, S. and Raj, K., 2018. DNA methylation-based biomarkers and the epigenetic clock theory of ageing. *Nature Reviews Genetics*, *19*(6), p.371.
(31)Goldstein, S., 1990. Replicative senescence: the human fibroblast comes of age. *Science*, *249*(4973), pp.1129-1133.
(32)Campisi, J., 1996. Replicative senescence: an old lives' tale?. *Cell*, *84*(4), pp.497-500.
(33)Shay, J.W. and Wright, W.E., 2000. Hayflick, his limit, and cellular ageing. *Nature reviews Molecular cell biology*, *1*(1), pp.72-76.
(34)Hayflick, L., 1965. The limited in vitro lifetime of human diploid cell strains. *Experimental cell research*, *37*(3), pp.614-636.
(35)Vandiver, A.R., Idrizi, A., Rizzardi, L., Feinberg, A.P. and Hansen, K.D., 2015. DNA methylation is stable during replication and cell cycle arrest. *Scientific reports*, *5*, p.17911.
(36)Brown, S.E., Fraga, M.F., Weaver, I.C., Berdasco, M. and Szyf, M., 2007. Variations in DNA methylation patterns during the cell cycle of HeLa cells. *Epigenetics*, *2*(1), pp.54-65.
(37)Desjobert, C., El Mai, M., Gérard-Hirne, T., Guianvarc'h, D., Carrier, A., Pottier, C., Arimondo, P.B. and Riond, J., 2015. Combined analysis of DNA methylation and cell cycle in cancer cells. *Epigenetics*, *10*(1), pp.82-91.
(38)Petkovich, D.A., Podolskiy, D.I., Lobanov, A.V., Lee, S.G., Miller, R.A. and Gladyshev, V.N., 2017. Using DNA methylation profiling to evaluate biological age and longevity interventions. *Cell metabolism*, *25*(4), pp.954-960.
(39)Thompson, M.J., Chwiałkowska, K., Rubbi, L., Lusis, A.J., Davis, R.C., Srivastava, A., Korstanje, R., Churchill, G.A., Horvath, S. and Pellegrini, M., 2018. A multi-tissue full lifespan epigenetic clock for mice. *Aging (Albany NY)*, *10*(10), p.2832.
(40)Cole, J.J., Robertson, N.A., Rather, M.I., Thomson, J.P., McBryan, T., Sproul, D., Wang, T., Brock, C., Clark, W., Ideker, T. and Meehan, R.R., 2017. Diverse interventions that extend mouse lifespan suppress shared age-associated epigenetic changes at critical gene regulatory regions. *Genome biology*, *18*(1), pp.1-16.
(41)Barwick, B.G., Scharer, C.D., Bally, A.P. and Boss, J.M., 2016. Plasma cell differentiation is coupled to division-dependent DNA hypomethylation and gene regulation. *Nature immunology*, *17*(10), pp.1216-1225.
(42)Rangarajan, A., Hong, S.J., Gifford, A. and Weinberg, R.A., 2004. Species-and cell type-specific requirements for cellular transformation. *Cancer cell*, *6*(2), pp.171-183.

This is a preliminary report of work that has not been certified by peer review.

(43)Franceschi, C., 1989. Cell proliferation, cell death and aging. *Aging Clinical and Experimental Research*, *1*(1), pp.3-15.
(44)von Wagenheim, K.H. and Peterson, H.P., 1998. Control of cell proliferation by progress in differentiation: clues to mechanisms of aging, cancer causation and therapy. *Journal of theoretical biology*, *193*(4), pp.663-678.
(45)Rojas, E., Herrera, L.A., Sordo, M., Gonsebatt, M.E., Montero, R., Rodriguez, R. and Ostrosky-Wegman, P., 1993. Mitotic index and cell proliferation kinetics for identification of antineoplastic activity. *Anti-Cancer Drugs*, *4*(6), pp.637-640
(46)Yang, Z., Wong, A., Kuh, D., Paul, D.S., Rakyan, V.K., Leslie, R.D., Zheng, S.C., Widschwendter, M., Beck, S. and Teschendorff, A.E., 2016. Correlation of an epigenetic mitotic clock with cancer risk. *Genome biology*, *17*(1), pp.1-18.
(47)Kim, B., Li, J., Jang, C. and Arany, Z., 2017. Glutamine fuels proliferation but not migration of endothelial cells. *The EMBO journal*, *36*(16), pp.2321-2333.
(48)Doronzo, G., Astanina, E., Corà, D., Chiabotto, G., Comunanza, V., Noghero, A., Neri, F., Puliafito, A., Primo, L., Spampanato, C. and Settembre, C., 2019. TFEB controls vascular development by regulating the proliferation of endothelial cells. *The EMBO journal*, *38*(3), p.e98250.
(49)Schiaffino, S., Dyar, K.A., Ciciliot, S., Blaauw, B. and Sandri, M., 2013. Mechanisms regulating skeletal muscle growth and atrophy. *The FEBS journal*, *280*(17), pp.4294-4314.
(50)Camarda, G., Siepi, F., Pajalunga, D., Bernardini, C., Rossi, R., Montecucco, A., Meccia, E. and Crescenzi, M., 2004. A pRb-independent mechanism preserves the postmitotic state in terminally differentiated skeletal muscle cells. *The Journal of cell biology*, *167*(3), pp.417-423.
(51)Li, L., Fu, Y.C., Xu, J.J., Chen, X.C., Lin, X.H. and Luo, L.L., 2011. Caloric restriction promotes the reproductive capacity of female rats via modulating the level of insulin-like growth factor-1 (IGF-1). *General and comparative endocrinology*, *174*(2), pp.232-237.
(52)Kari, F.W., Dunn, S.E., French, J.E. and Barrett, J.C., 1999. Roles for insulin-like growth factor-1 in mediating the anti-carcinogenic effects of caloric restriction. *The journal of nutrition, health & aging*, *3*(2), pp.92-101.
(53)López-Otín, C., Galluzzi, L., Freije, J.M., Madeo, F. and Kroemer, G., 2016. Metabolic control of longevity. *Cell*, *166*(4), pp.802-821.
(54)Acosta-Rodríguez, V.A., de Groot, M.H., Rijo-Ferreira, F., Green, C.B. and Takahashi, J.S., 2017. Mice under caloric restriction self-impose a temporal restriction of food intake as revealed by an automated feeder system. *Cell metabolism*, *26*(1), pp.267-277.
(55)Chaix, A., Zarrinpar, A., Miu, P. and Panda, S., 2014. Time-restricted feeding is a preventative and therapeutic intervention against diverse nutritional challenges. *Cell metabolism*, *20*(6), pp.991-1005.
(56)Zheng, Z., Li, C., Ha, P., Chang, G.X., Yang, P., Zhang, X., Kim, J.K., Jiang, W., Pang, X., Berthiaume, E.A. and Mills, Z., 2019. CDKN2B upregulation prevents teratoma formation in multipotent fibromodulin-reprogrammed cells. *Journal of Clinical Investigation*, *129*(8), pp.3236-3251.
(57)Olova, N., Simpson, D.J., Marioni, R.E. and Chandra, T., 2019. Partial reprogramming induces a steady decline in epigenetic age before loss of somatic identity. *Aging cell*, *18*(1), p.e12877.
(58)Gil, J., Bernard, D., Martínez, D. and Beach, D., 2004. Polycomb CBX7 has a unifying role in cellular lifespan. *Nature cell biology*, *6*(1), pp.67-72.
(59)Forzati, F., Federico, A., Pallante, P., Abbate, A., Esposito, F., Malapelle, U., Sepe, R., Palma, G., Troncone, G., Scarfò, M. and Arra, C., 2012. CBX7 is a tumor suppressor in mice and humans. *The Journal of clinical investigation*, *122*(2).
(60)Li, Q., Wang, X., Lu, Z., Zhang, B., Guan, Z., Liu, Z., Zhong, Q., Gu, L., Zhou, J., Zhu, B. and Ji, J., 2010. Polycomb CBX7 directly controls trimethylation of histone H3 at lysine 9 at the p16 locus. *PloS one*, *5*(10), p.e13732.
(61)Su, W.J., Fang, J.S., Cheng, F., Liu, C., Zhou, F. and Zhang, J., 2013. RNF2/Ring1b negatively regulates p53 expression in selective cancer cell types to promote tumor development. *Proceedings of the National Academy of Sciences*, *110*(5), pp.1720-1725.
(62)Wilting, R.H., Yanover, E., Heideman, M.R., Jacobs, H., Horner, J., Van Der Torre, J., DePinho, R.A. and Dannenberg, J.H., 2010. Overlapping functions of Hdac1 and Hdac2 in cell cycle regulation and haematopoiesis. *The EMBO journal*, *29*(15), pp.2586-2597.

This is a preliminary report of work that has not been certified by peer review.

(63)Wilkinson, J.E., Burmeister, L., Brooks, S.V., Chan, C.C., Friedline, S., Harrison, D.E., Hejtmancik, J.F., Nadon, N., Strong, R., Wood, L.K. and Woodward, M.A., 2012. Rapamycin slows aging in mice. *Aging cell*, *11*(4), pp.675-682.
(64)Barwick, B.G., Scharer, C.D., Martinez, R.J., Price, M.J., Wein, A.N., Haines, R.R., Bally, A.P., Kohlmeier, J.E. and Boss, J.M., 2018. B cell activation and plasma cell differentiation are inhibited by de novo DNA methylation. *Nature communications*, *9*(1), pp.1-14.
(65)Levine, M.E., Leung, D., Minteer, C. and Gonzalez, J., 2019. A DNA Methylation Fingerprint of Cellular Senescence. *bioRxiv*, p.674580.
(66)Serrano, M., Lin, A.W., McCurrach, M.E., Beach, D. and Lowe, S.W., 1997. Oncogenic ras provokes premature cell senescence associated with accumulation of p53 and p16INK4a. *Cell*, *88*(5), pp.593-602.
(67)Harvey, M., Sands, A.T., Weiss, R.S., Hegi, M.E., Wiseman, R.W., Pantazis, P., Giovanella, B.C., Tainsky, M.A., Bradley, A. and Donehower, L.A., 1993. In vitro growth characteristics of embryo fibroblasts isolated from p53-deficient mice. *Oncogene*, *8*(9), p.2457.
(68)Kamijo, T., Zindy, F., Roussel, M.F., Quelle, D.E., Downing, J.R., Ashmun, R.A., Grosveld, G. and Sherr, C.J., 1997. Tumor suppression at the mouse INK4a locus mediated by the alternative reading frame product p19 ARF. *Cell*, *91*(5), pp.649-659.
(69)Lin, W., Cao, J., Liu, J., Beshiri, M.L., Fujiwara, Y., Francis, J., Cherniack, A.D., Geisen, C., Blair, L.P., Zou, M.R. and Shen, X., 2011. Loss of the retinoblastoma binding protein 2 (RBP2) histone demethylase suppresses tumorigenesis in mice lacking Rb1 or Men1. *Proceedings of the National Academy of Sciences*, *108*(33), pp.13379-13386.
(70)Pear, W.S., Nolan, G.P., Scott, M.L. and Baltimore, D., 1993. Production of high-titer helper-free retroviruses by transient transfection. *Proceedings of the National Academy of Sciences*, *90*(18), pp.8392-8396.
(71)Nolan Laboratory Retroviral Systems. Phoenix helper-free retrovirus producer lines, https://web.stanford.edu/group/nolan/_OldWebsite/retroviral_systems/retsys.html

This is a preliminary report of work that has not been certified by peer review.